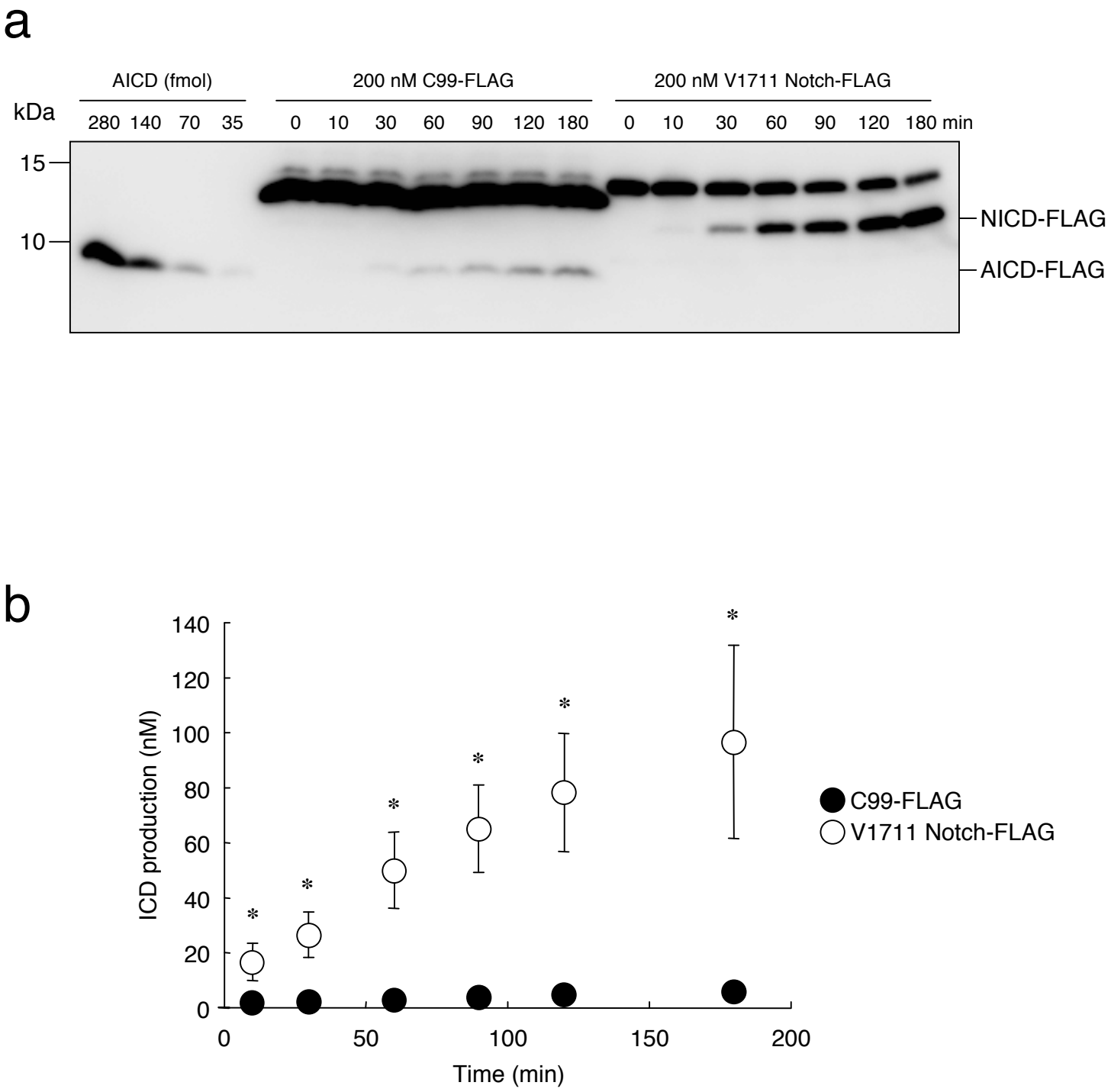

Supplementary Figure S1. Time-dependent production of ICDs from γ-secretase substrates. γ-Secretase substrates (200 nM C99-FLAG or 200 nM V1711 Notch-FLAG) were incubated with a γ-secretase fraction at 37˚C. The reaction was terminated at the time indicated by placing the reaction tube on ice. ICD-FLAG fragments produced, together with authentic AICD-FLAG, were separated on a gel, and followed by Western blotting with anti-FLAG M2 antibody (**a**). AICD-FLAG and NICD-FLAG were produced in a time-dependent manner. The volume of C99-FLAG reaction loaded onto the gel was sevenfold more than that of V1711 Notch-FLAG reaction. Data represent means ± SD of three independent experiments (**b**). *$P < 0.05$ (unpaired t-test).

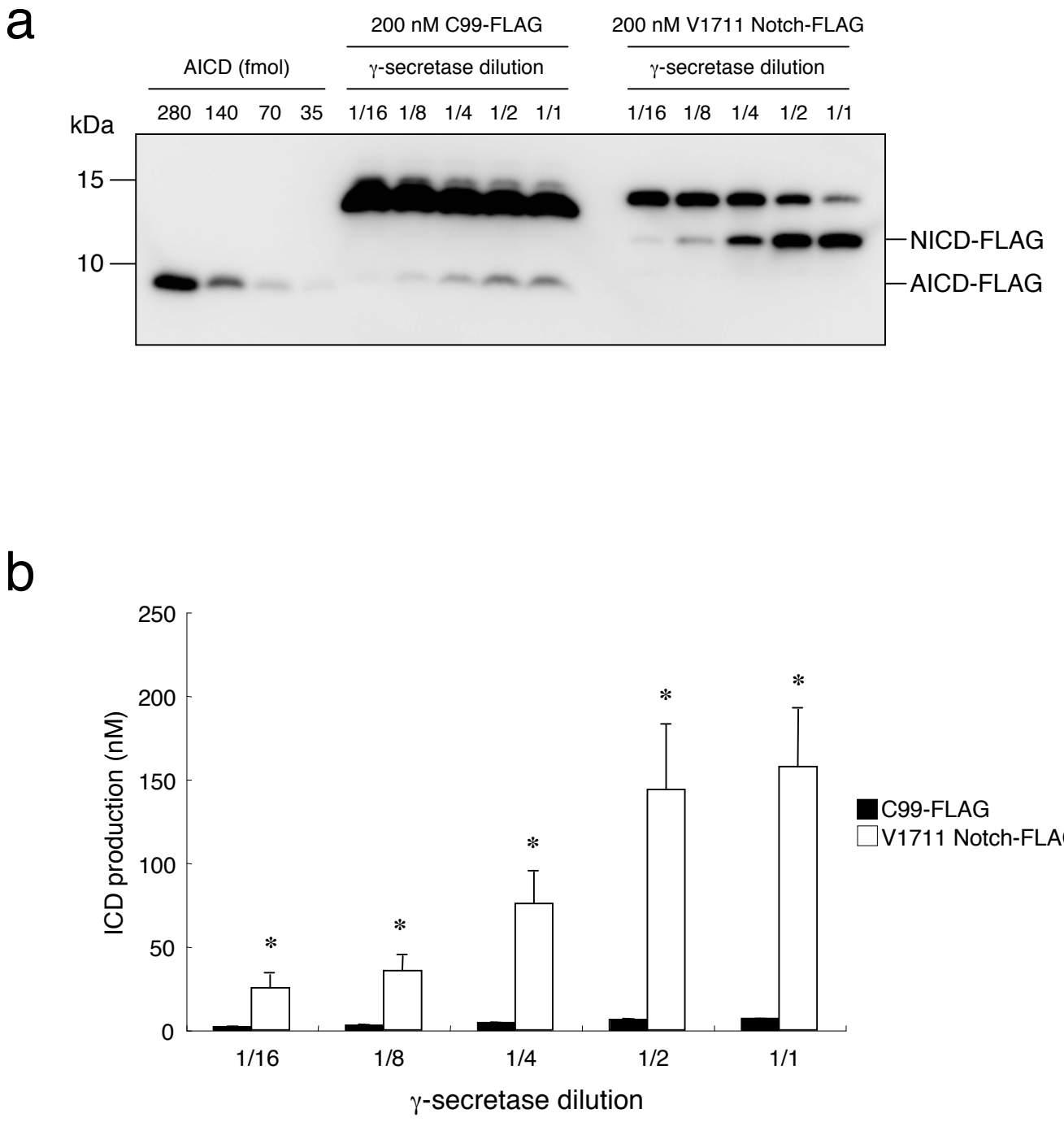

Supplementary Figure S2. γ-Secretase dose-dependent production of ICDs from their substrates. γ-Secretase substrates (200 nM C99-FLAG or 200 nM V1711 Notch-FLAG) were incubated with serial dilutions of a γ-secretase fraction at 37˚C for 4 h. ICD-FLAG fragments produced, together with authentic AICD-FLAG, were separated on a gel, followed by Western blotting with anti-FLAG M2 antibody (**a**). AICD-FLAG and NICD-FLAG were produced in a γ-secretase dose-dependent manner. The volume of C99-FLAG reaction loaded onto the gel was sevenfold more than that of the V1711 Notch-FLAG reaction. Data represent means ± SD of three independent experiments (**b**). *$P < 0.05$ (unpaired t-test).

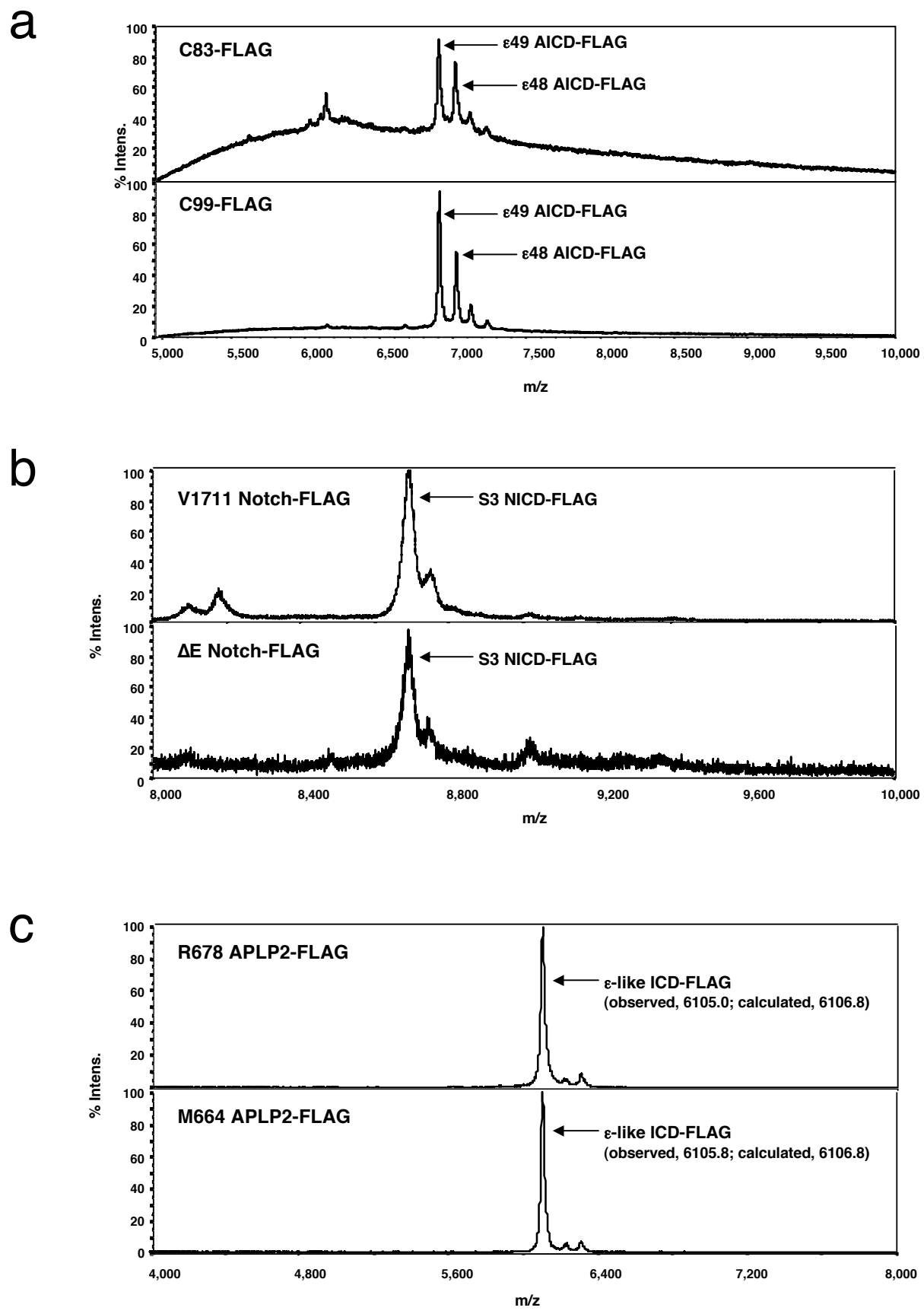

Supplementary Figure S3. Ectodomain length did not affect ε, S3, or ε-like cleavage sites. γ-Secretase substrates were incubated with a γ-secretase fraction. The intracellular domain released from the substrates was immunoprecipitated with anti-FLAG M2 agarose beads and analysed by mass spectrometry (**a,** C83-FLAG and C99-FLAG; **b,** V1711 Notch-FLAG and ΔE Notch-FLAG; **c,** R678 APLP2-FLAG and M664 APLP2-FLAG). Ectodomain length did not alter cleavage sites in substrates tested in this study.

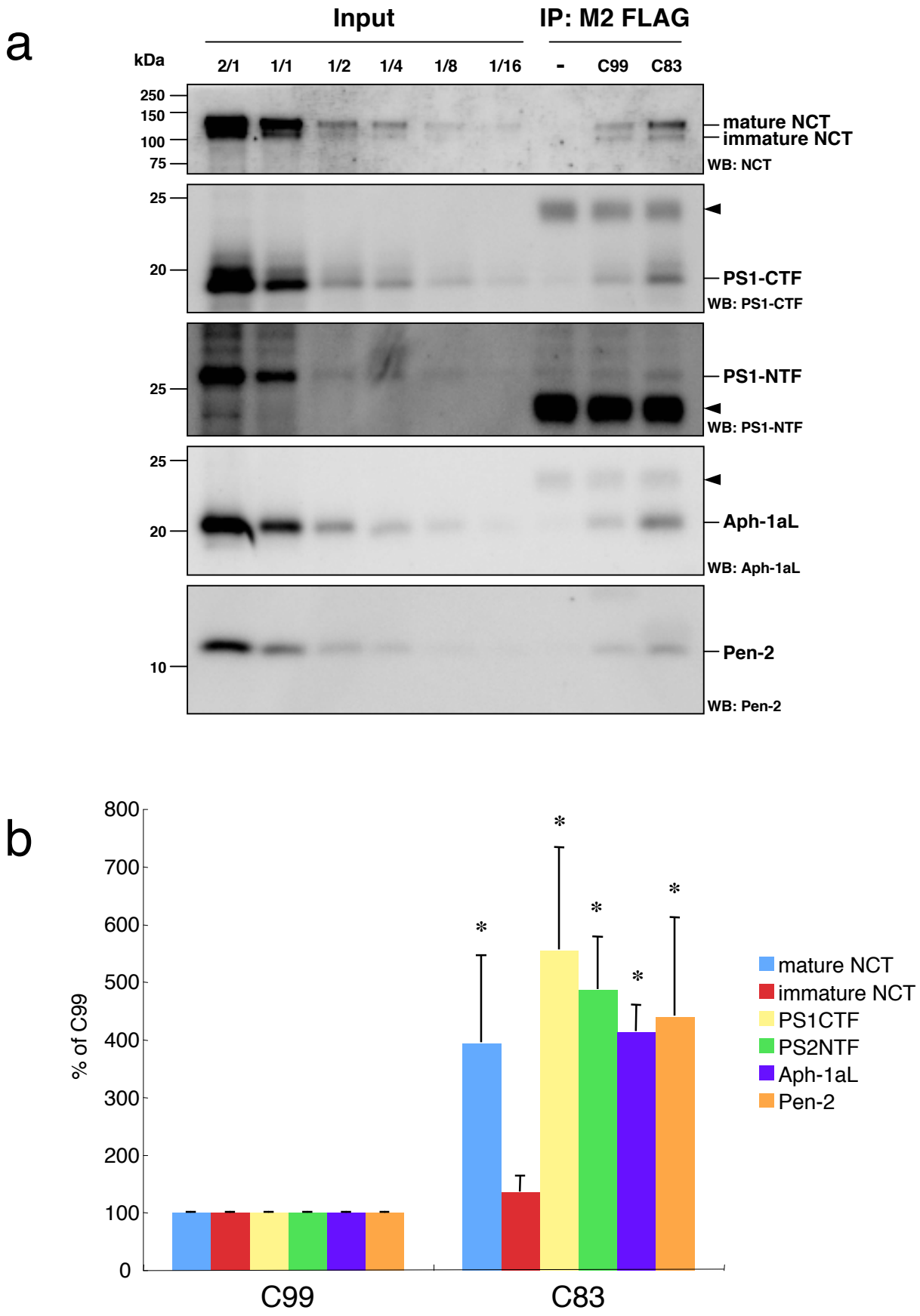

Supplementary Figure S4. Interaction between γ-secretase and substrate. γ-Secretase substrates (C83-FLAG or C99-FLAG) were immobilized using anti-FLAG M2 magnetic beads and mixed with a γ-secretase fraction at 4˚C. After sufficient washing of co-immunoprecipitates, Western blotting was used to visualize and quantify γ-secretase components. C83-FLAG had an increased interaction with γ-secretase components compared with C99-FLAG. Arrow heads indicate the position of IgG used for co-immunoprecipitation (**a**). Data are expressed as means ± SD of three independent experiments (**b**). *$P < 0.05$ (unpaired t-test).

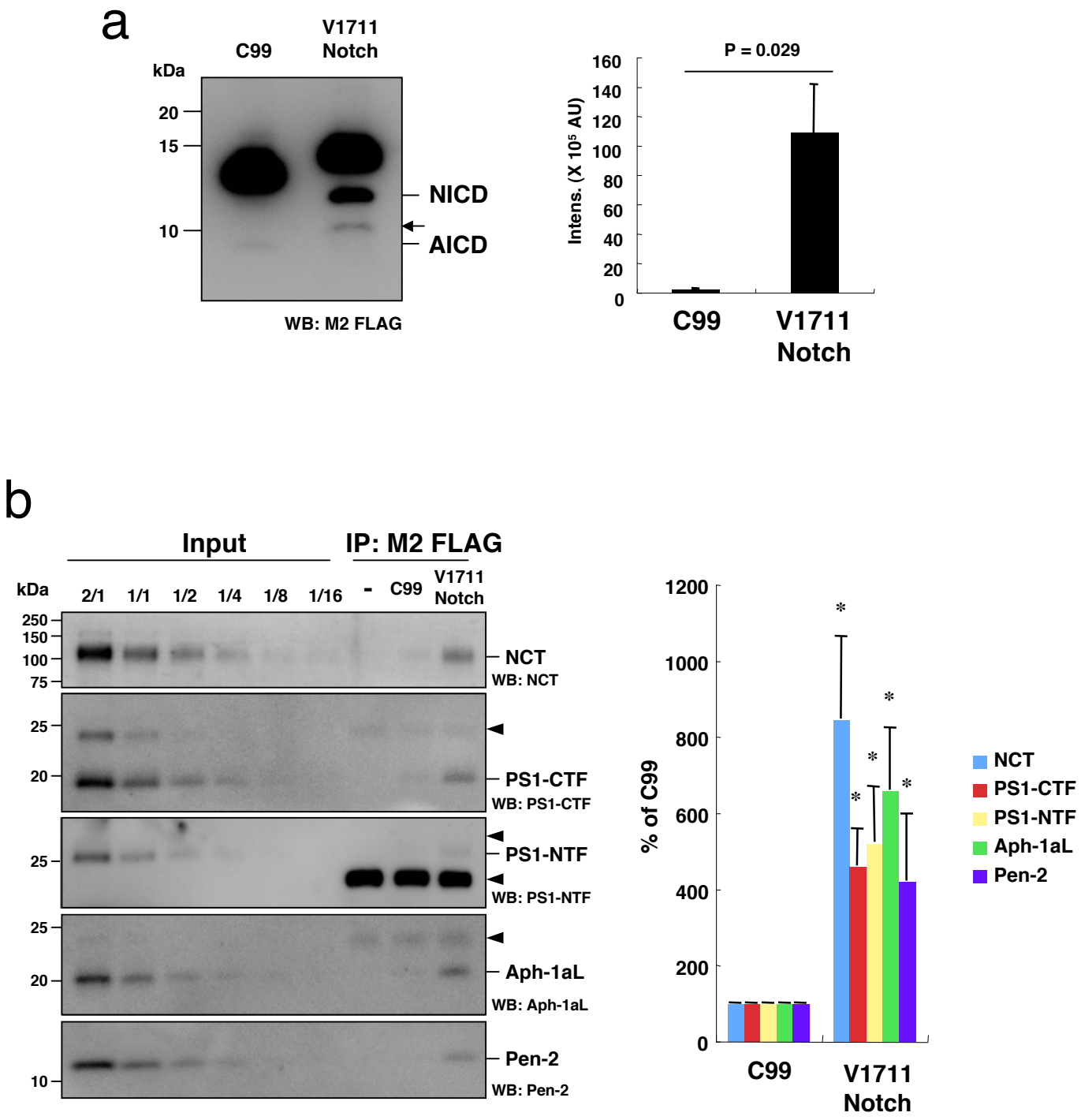

Supplementary Figure S5. Substrate preference of γ-secretase from human brain. γ-Secretase substrates were incubated with a γ-secretase fraction from human brain. The intracellular domain released from the substrates was detected with anti-FLAG M2 antibody. Human brain γ-secretase exhibited preferential cleavage of V1711 Notch substrate (**a**). Arrow indicates degradation product of V1711 Notch during purification. Data are expressed as means ± SD of three independent experiments. *$P < 0.05$ (unpaired t-test). Substrates were immobilized using anti-FLAG M2 magnetic beads and mixed with γ-secretase fractions of the human brain (**b**). After sufficient washing of co-immunoprecipitates, Western blotting was used to visualize and quantify γ-secretase components. V1711 Notch-FLAG had an increased interaction with γ-secretase components compared with C99-FLAG. Arrow heads indicate the position of IgG used for co-immunoprecipitation. Data are expressed as means ± SD of three independent experiments. *$P < 0.05$ (unpaired t-test).

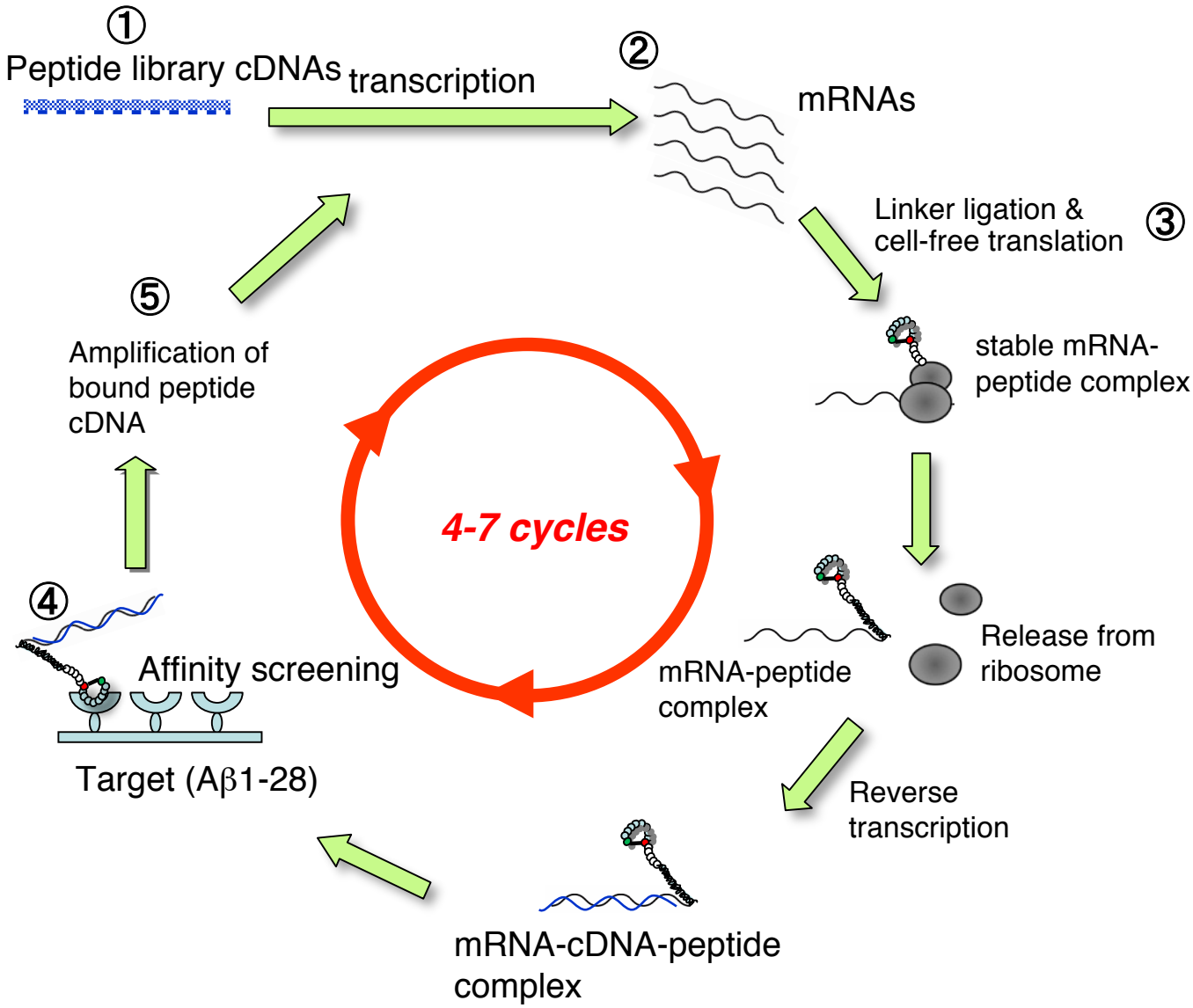

Supplementary Figure S6. Schematic diagram of peptide display. A DNA library was constructed from synthetic oligonucleotides, which included ATG(NNT)$_{20}$ or ATG(NNK)$_{20}$ (N is A, C, G, or T, and K is G or T) as a randomized peptide-encoding region. The NNT-type was added in the same amount as the NNK-type to increase the proportion of Cys and Tyr and to decrease the appearance of stop codons (step 1). The DNA library was subjected to transcription (step 2) and the resultant mRNA library was employed as a template for a covalently linked peptide (step 3). After reverse transcription, peptide-displaying molecules were incubated with Aβ1−28 immobilized (step 4). After washing the beads, the binding molecules were recovered by heating and subjected to PCR to prepare templates for the next round of amplification (step 5).

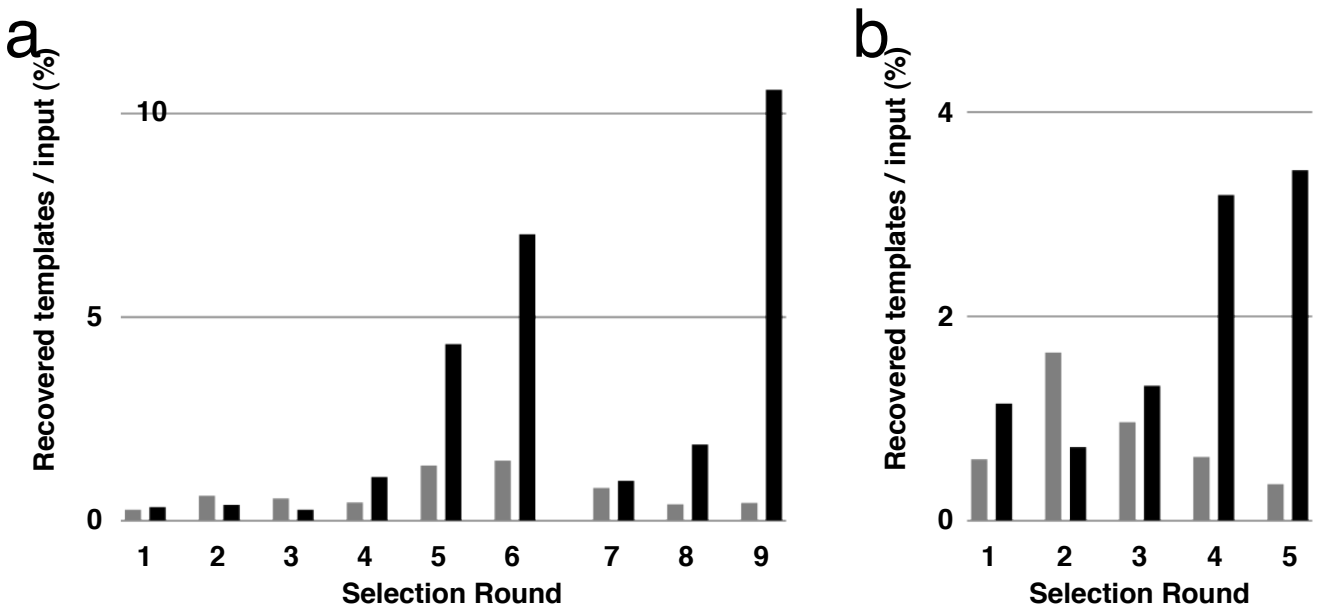

c

9-7	MNYLICDCYCSLTRCFCYSCVDS
6-5	MHHVYCDCYCFGPVCYCHSCT
9-6	MPHCVFGVLCDRLRCRRGWLC
9-4	MRGHLCLCNGDLCRCYHGFLY
9-5	MLCVRGWMLPSRQYGKLCLMD
9-8	MLCEWHSVPRGWLCLVPQFHG
9-1	MVFCYPVNAHAFVCDIYSIRY
6-4	MFESCYPFWWGRYCYSVHSKL
9-3	MRGMLCDLYGRCMRGILVYLP
6-1	MWLPFLFKMWMLMFFAQLSIS
6-2	MVYYRWTHRNAYLSYDYAWMM
6-3	MVPWMMLLVLMSYISVLRGLM

Supplementary Figure S7. Selection of binding peptides. Templates of peptide-displaying molecules were quantified by real-time PCR after reverse transcription of mRNA (**a**). The concentration of Aβ1−28-binding molecules was estimated by comparing the ratio of templates recovered from biotinyl-Aβ1−28-immobilized streptavidin beads to input (black bars) with the ratio of templates from biotin-bound streptavidin beads to input (grey bars). At the seventh round of selection, bait concentration was decreased from 2.6 μM to 0.65 μ M to obtain high-affinity C99-binding peptides. Peptide-displaying molecules from the semi-random library designed from peptides 6-5 and 9-7 were incubated with 0.65 μM bait for 1 h at 37°C, instead of the ambient temperature of the initial selection, and the proceeding selection was monitored in the same manner as the initial selection (**b**). The templates after the sixth and ninth rounds were cloned and their sequences were determined (**c**). Peptides 6-1 to 6-5 were derived from the sixth round and 9-1 to 9-7 are from the ninth round. Cys is highlighted with red. Sequences from the semi-random library are listed in Figure 3a.

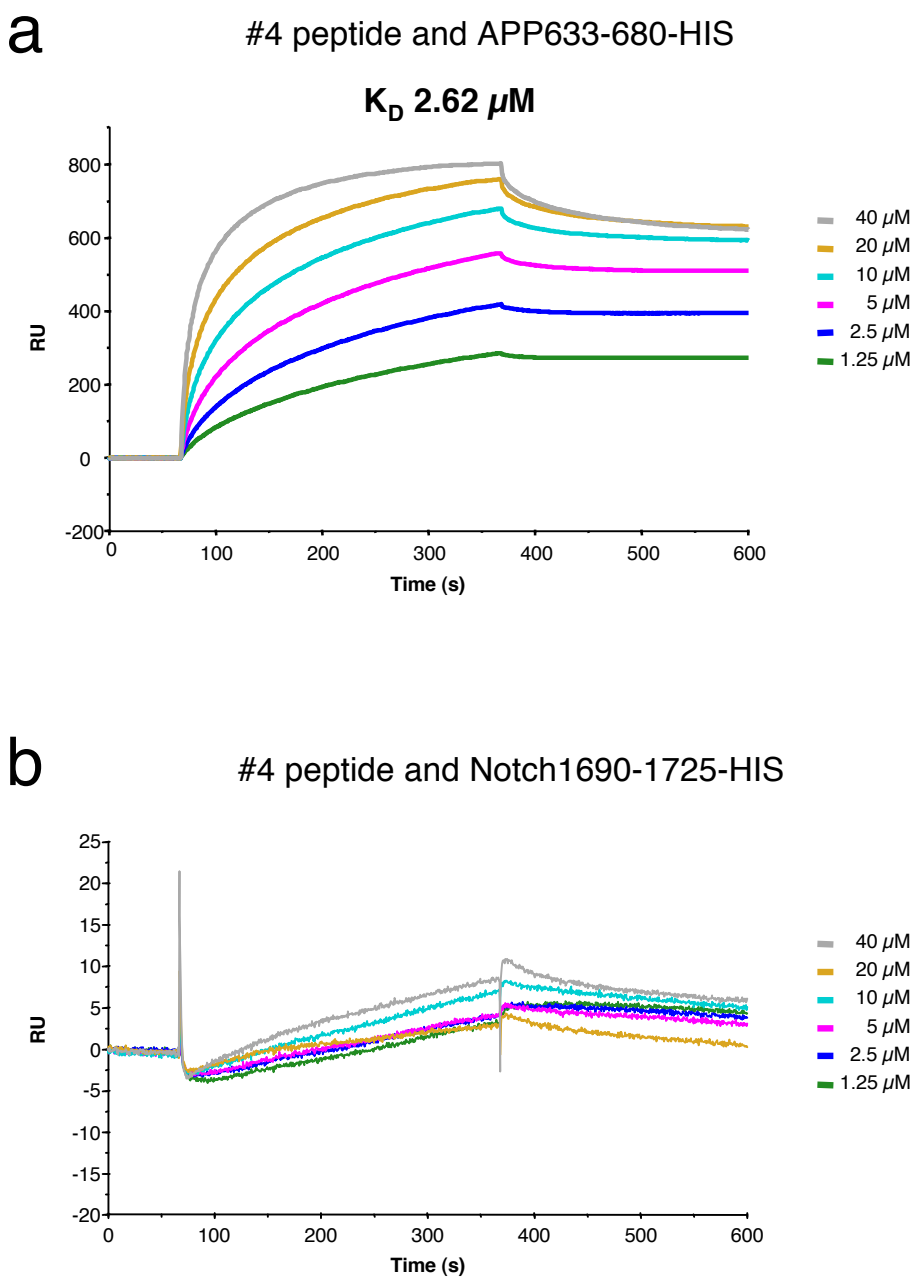

Supplementary Figure S8. BIACORE analysis on peptide #4. Association and dissociation curves are shown for binding of immobilized target fragments to peptide #4 at the concentration indicated for 360 s then dissociated for 240 s. Peptide #4 with APP633-680 had an affinity of approximately 2.62 μM (**a**). #4 peptide showed no appreciable binding to Notch1690-1725 (**b**).

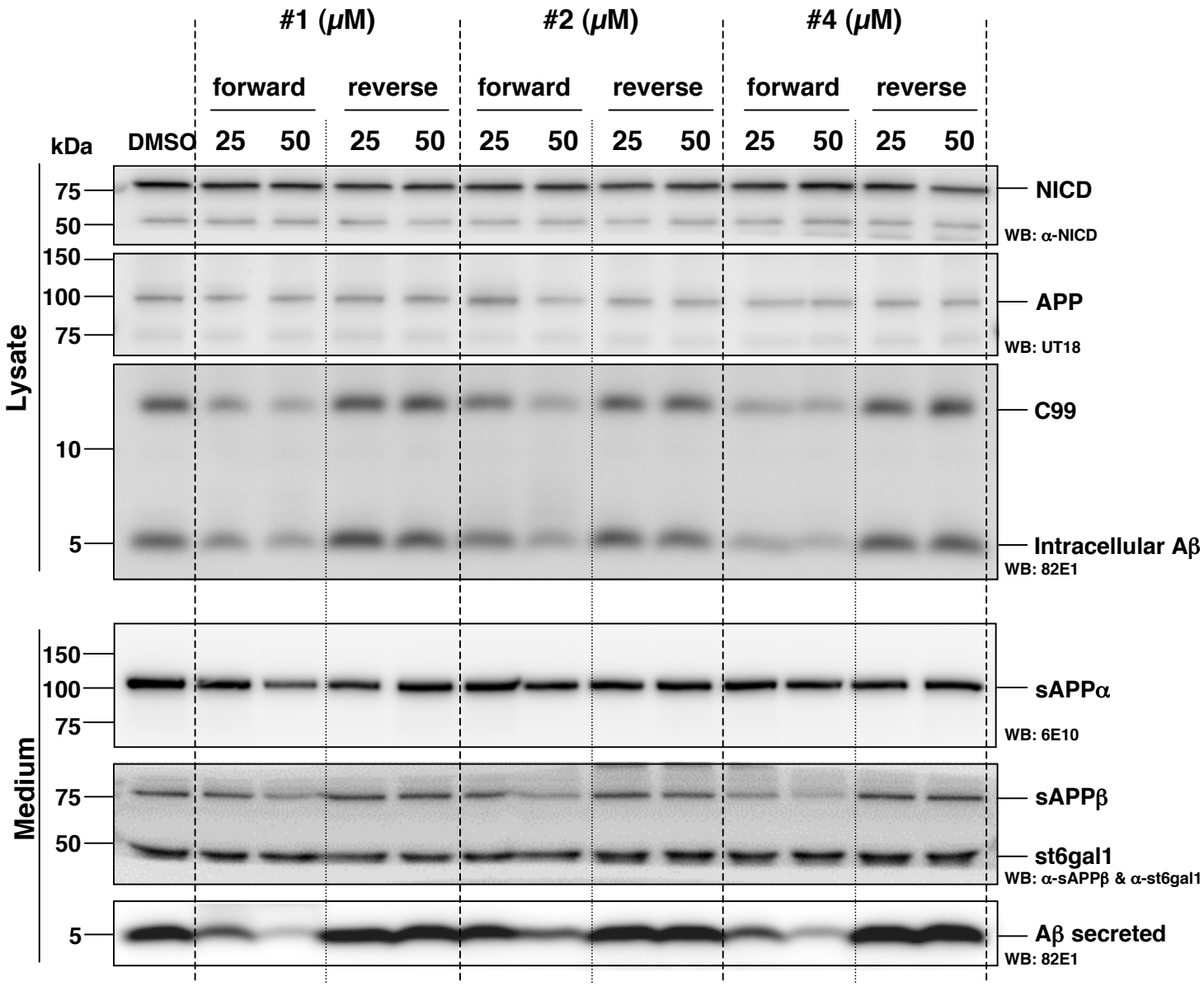

Supplementary Figure S9. The C99-binding peptides reduced Aβ, C99 and sAPPβ production, but failed to suppress Notch and St6gal1 cleavages. 7WD10 cells co-expressing Notch and St6gal1 were treated with the C99-binding peptides (forward or reverse sequence) for 2 days (see full methods). Levels of Aβ, C99 and sAPPβ were reduced by the C99-binding peptides without interfering with sAPPα production and Notch and St6gal1 cleavage. However, the reverse peptides failed to suppress productions of Aβ, C99 and sAPPβ.

a

b

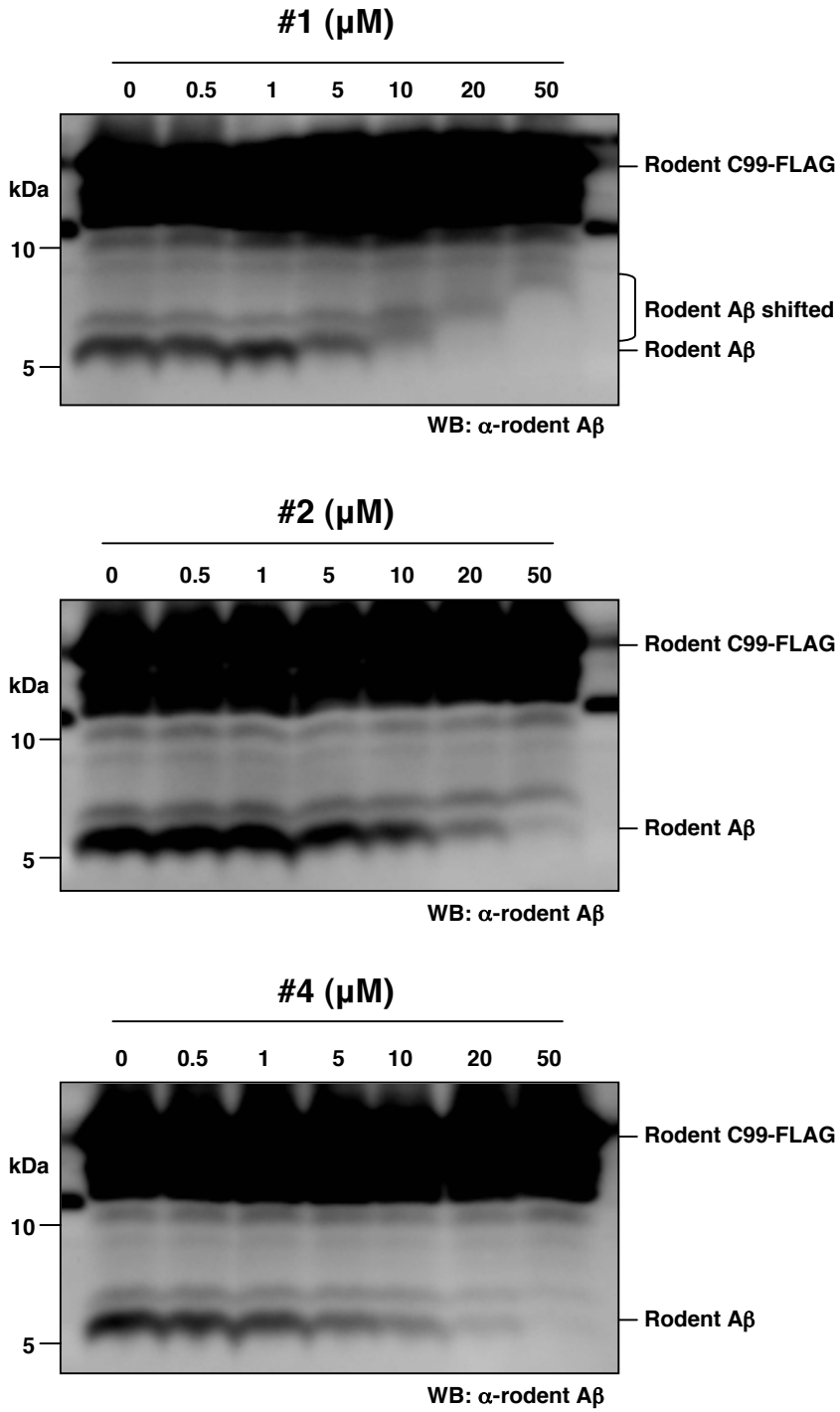

Supplementary Figure S10. C99-binding peptides inhibited production of Aβ from rodent C99-FLAG substrate in a dose dependent manner. C99-FLAG substrate containing rodent substitutions was generated (**a**). Rodent C99-FLAG was incubated with a γ-secretase fraction in the presence of C99-binding peptides (**b**). Rodent Aβ production was visualized by using anti-rodent Aβ antibody. C99-binding peptides inhibited Aβ production even from rodent C99-FLAG in a dose dependent manner. Peptide #1 retarded Aβ migration as shown in Fig. 4b and Fig. 5b.

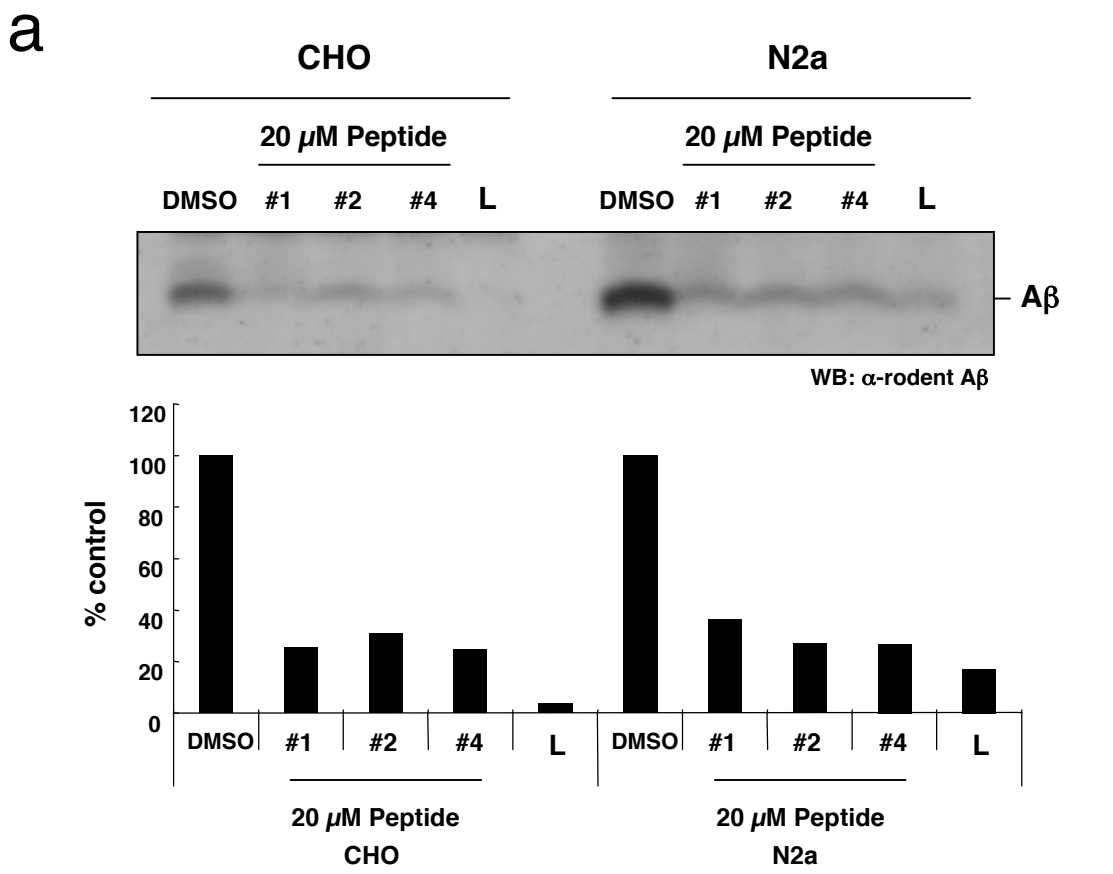

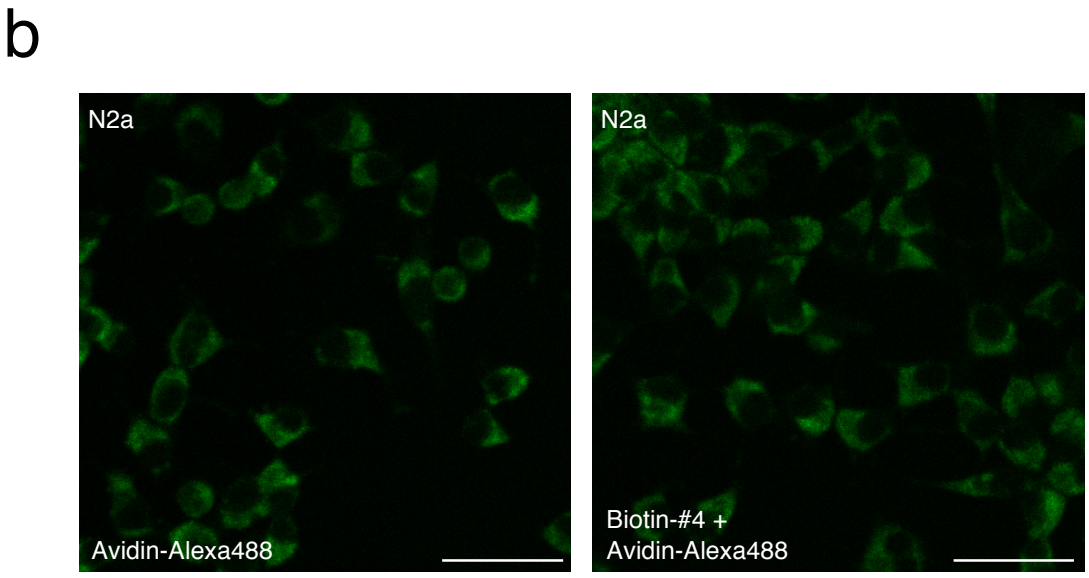

Supplementary Figure S11. C99-binding peptides suppressed production of rodent endogenous Aβ in CHO and Neuro 2a cells. CHO and Neuro 2a (N2a) cells were cultivated in the presence or absence of C99-binding peptides in an animal-component-free medium, CD-AF (Sigma), to avoid detection of Aβ in serum that would confound results (**a**). Conditioned media were incubated with 4G8 antibody to immunoprecipitate endogenous rodent Aβ, which was determined by Western blotting with anti-rodent Aβ antibody (IBL). All C99-binding peptides reduced production of the endogenous rodent Aβ. This demonstrates that the C99-binding peptides are able to suppress even rodent Aβ production. L, 1 μM L-685,458. N2a cells were treated with biotinylated peptide #4 (**b**). Fixed and permeabilized cells were stained using streptavidin–Alexa488. No significant staining difference was observed between N2a cells treated with Bio-#4/Avidin-Alexa488 and those treated with Alexa488 alone. It is likely that the endogenous APP level in N2a cells was lower than that in 7WD10 as shown in Figure 6b. In addition to this, affinity of #4 peptide was not as high as conventional anti-Aβ antibodies. Bar, 50 μm.

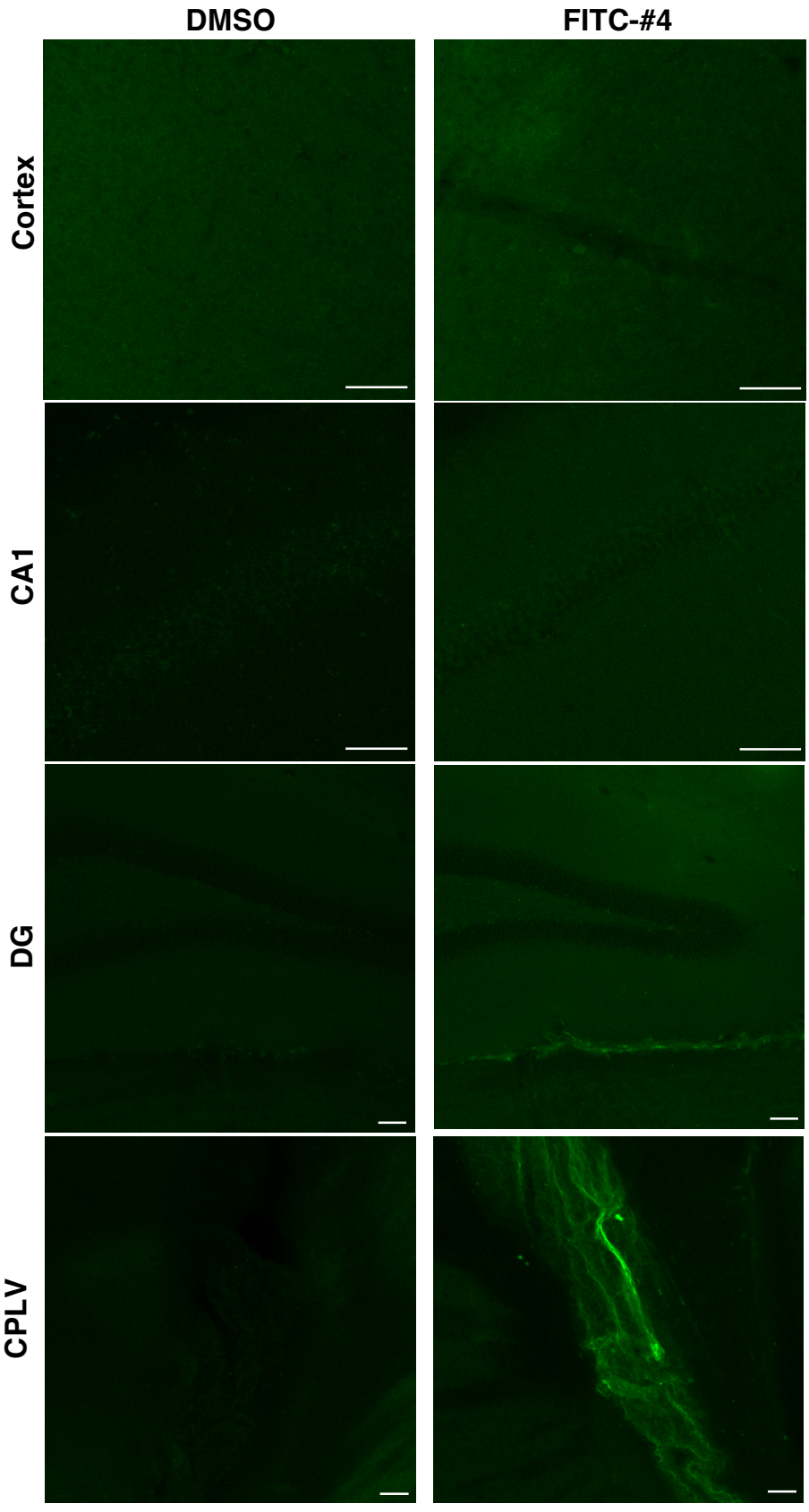

Supplementary Figure S12. C99-binding peptides in the brain. Faint fluorescence from the peptide was observed in the cortex, hippocampus (CA1 and DG), and choroid plexus of the lateral ventricle (CPLV) of mice administered with the peptide, but not in those treated with DMSO. It seems reasonable to suppose that a certain amount of the peptide penetrates the blood brain barrier into the brain, although FITC-labelled peptide #4 was not detected in individual neurons. Even if the peptide was incorporated into neurons of treated mice, it may be difficult to detect the peptide because of the low level of expression of endogenous APP in neurons and insufficient affinity of the peptide for APP, as in the case of N2a cells shown in Supplementary Fig. S13. Bar, 50 μm.

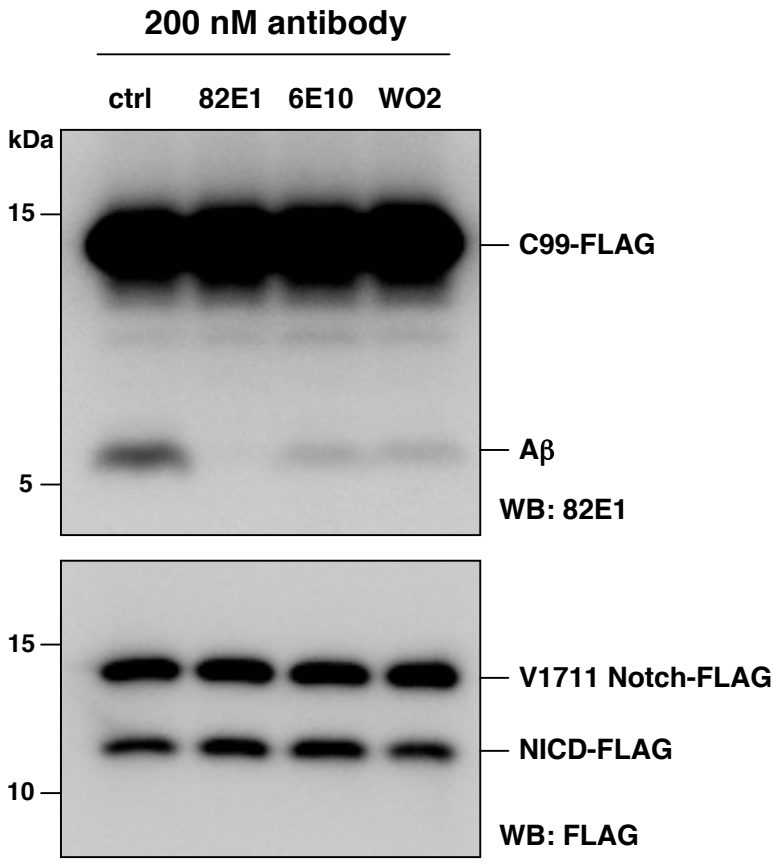

Supplementary Figure S13. WO2 antibody suppressed Aβ production. C99-FLAG substrate (50 nM) was incubated with CHAPSO-solubilized γ-secretase in the presence of 200 nM WO2 antibody raised against the amino terminus of Aβ. WO2 exhibited suppression of Aβ production, but had no effect on Notch cleavage, as do antibodies 82E1 and 6E10.

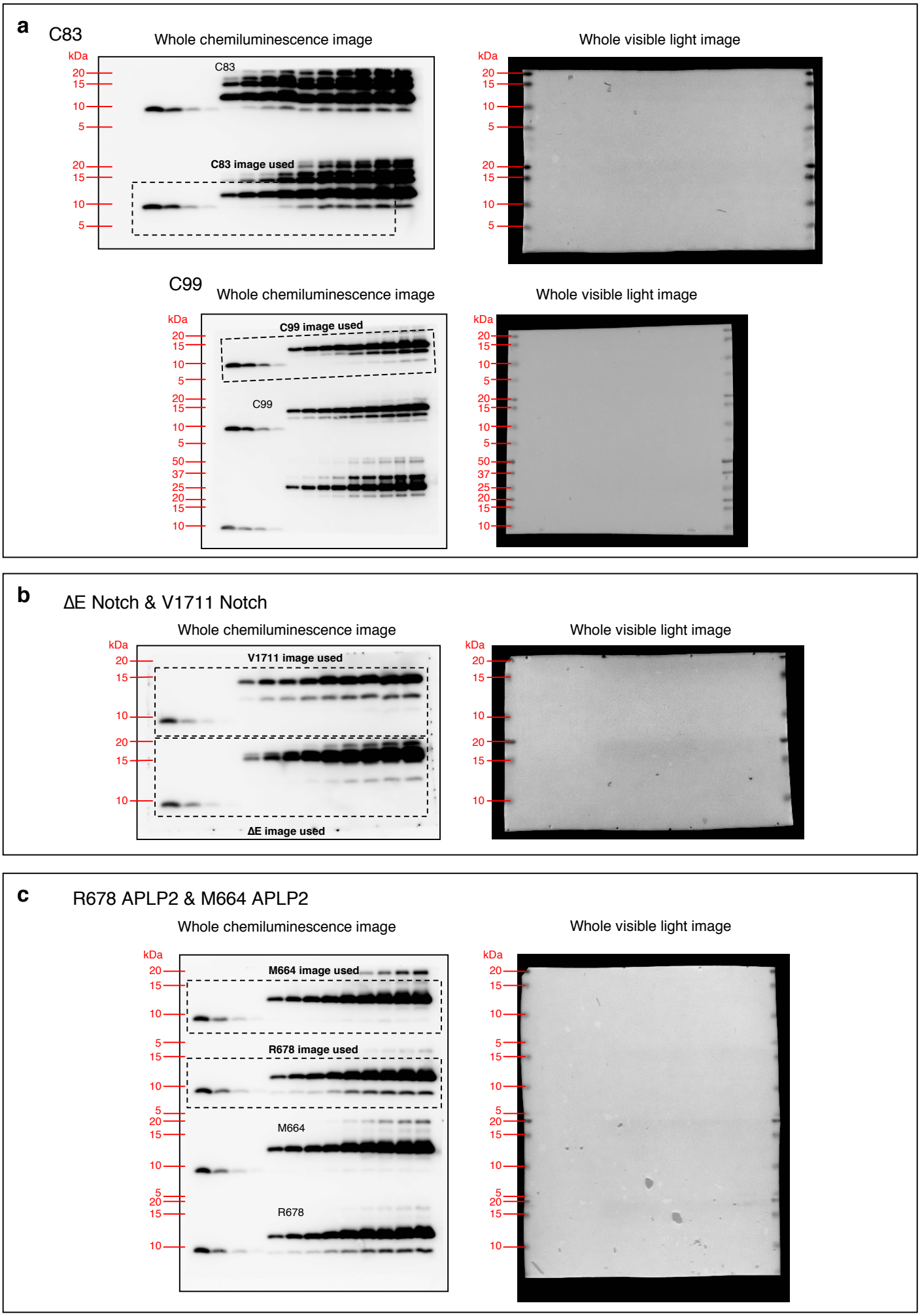

Supplementary Figure S14. Full scan images of Figure 2. Dashed rectangles indicate area used in Figure 2.

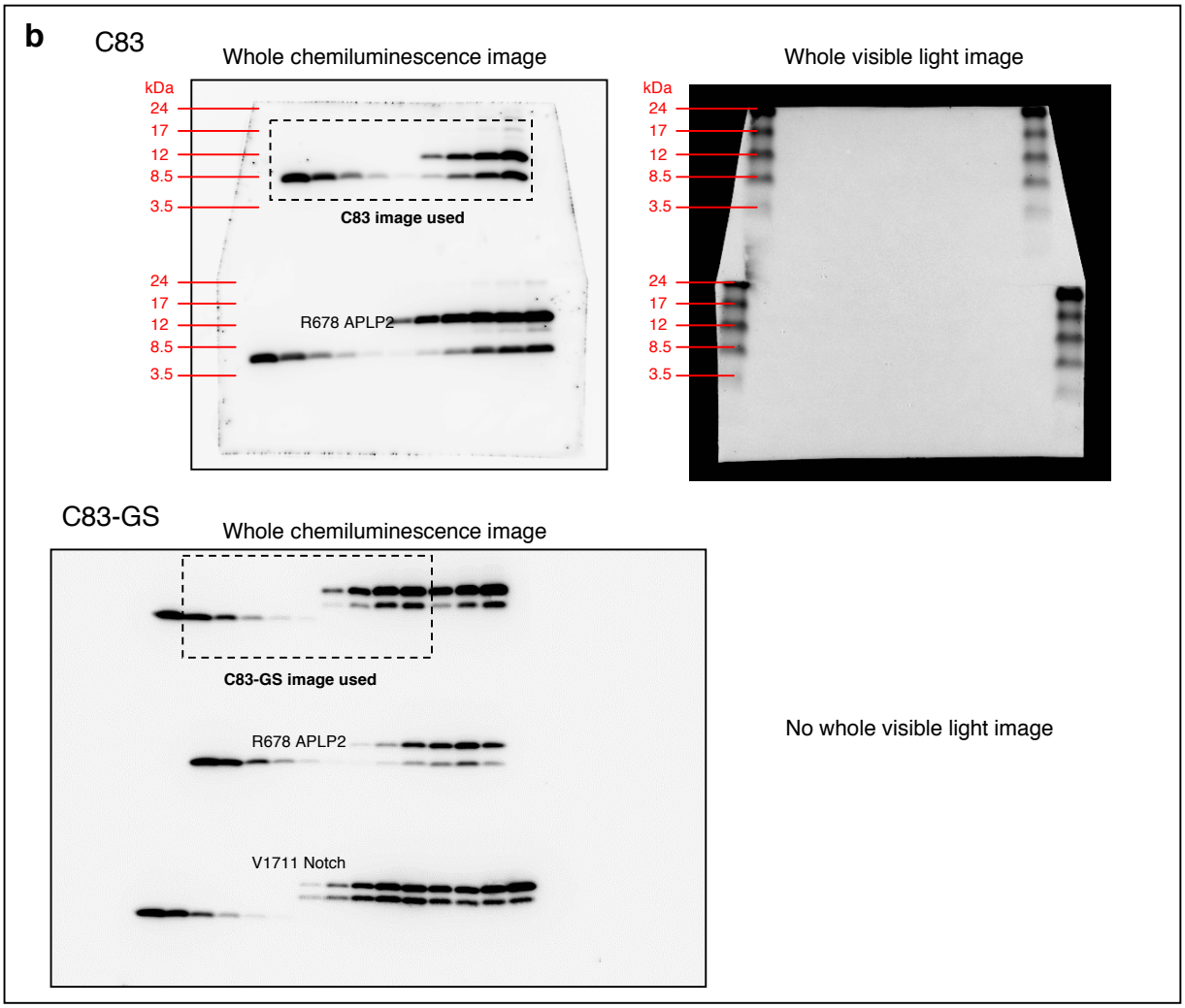

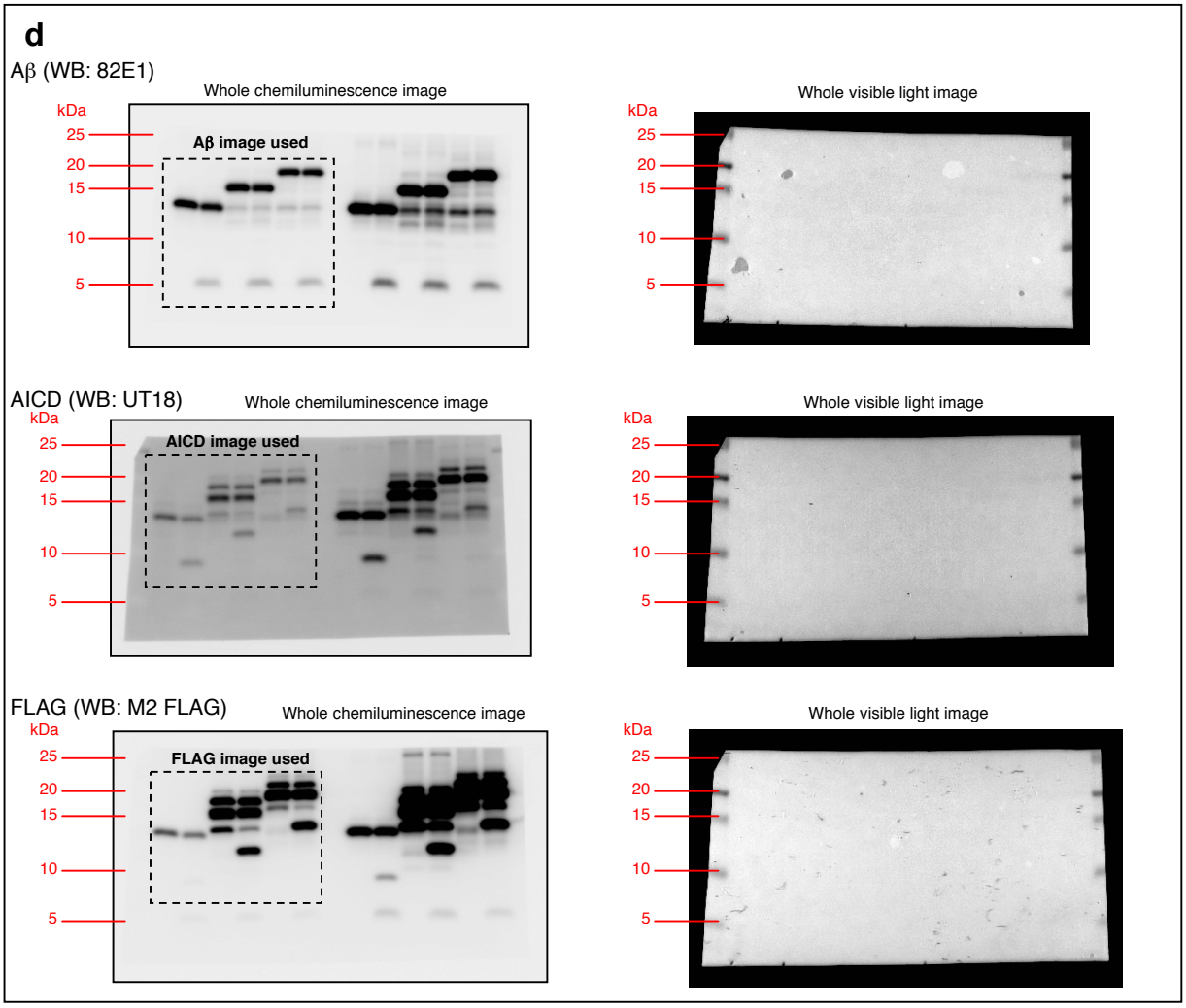

Supplementary Figure S15. Full scan images of Figure 3. Dashed rectangles indicate area used in Figure 3.

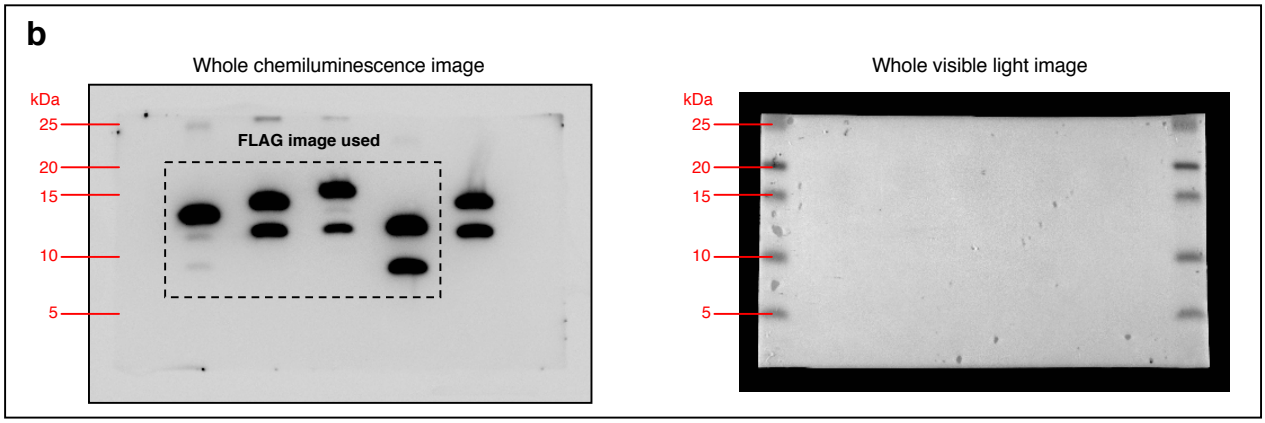

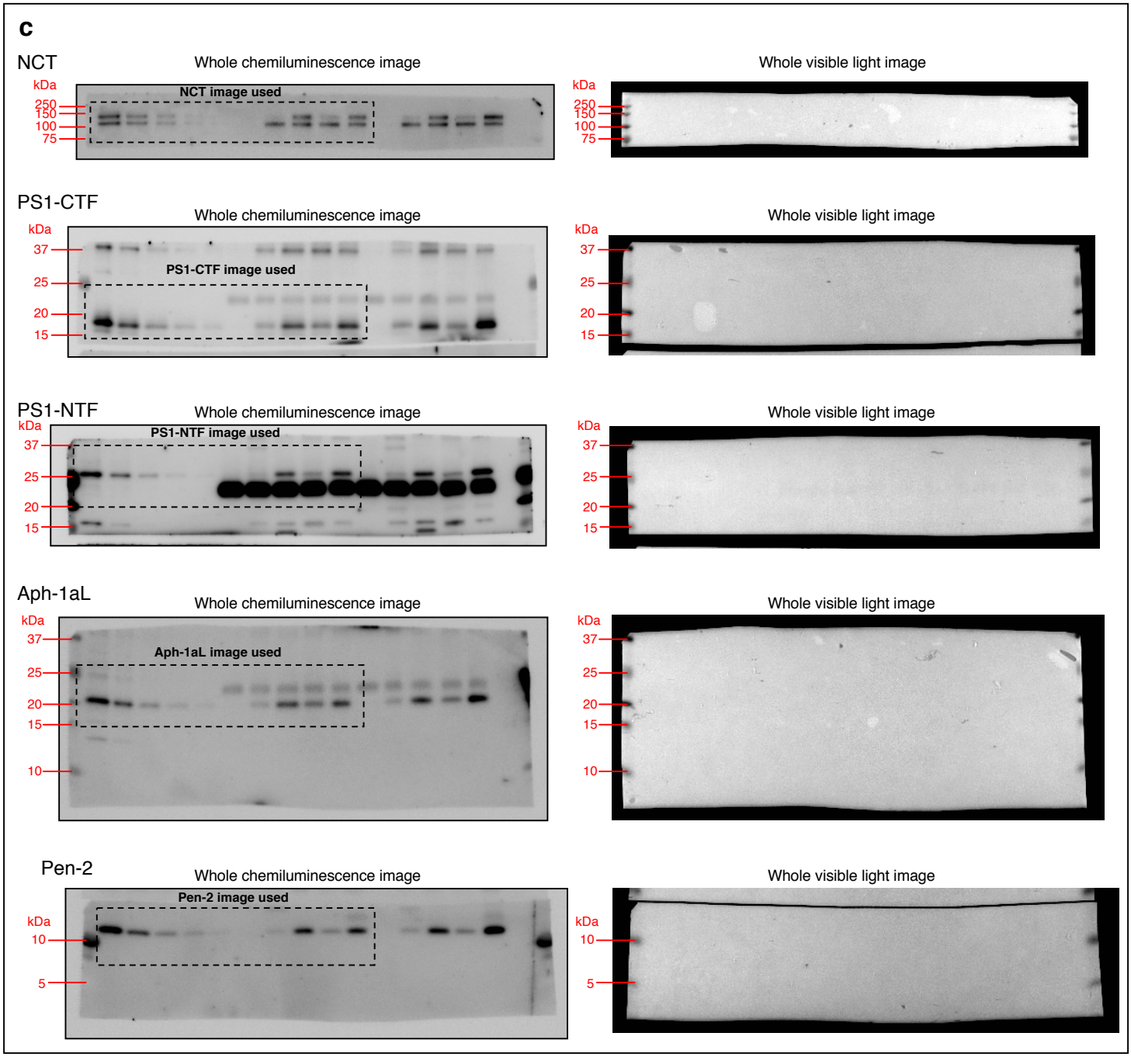

Supplementary Figure S16. Full scan images of Figure 4. Dashed rectangles indicate area used in Figure 4.

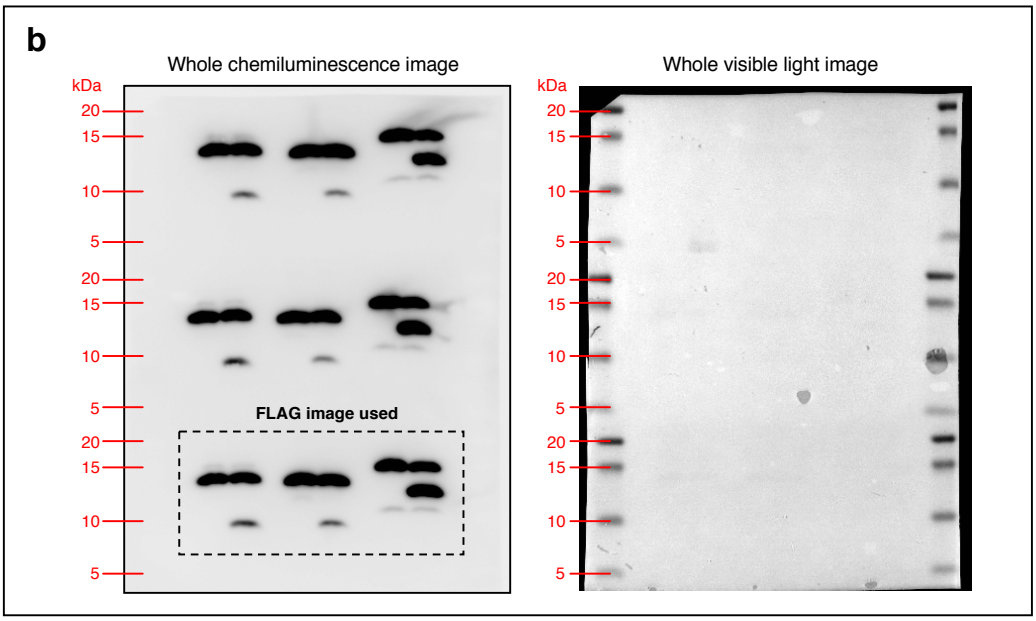

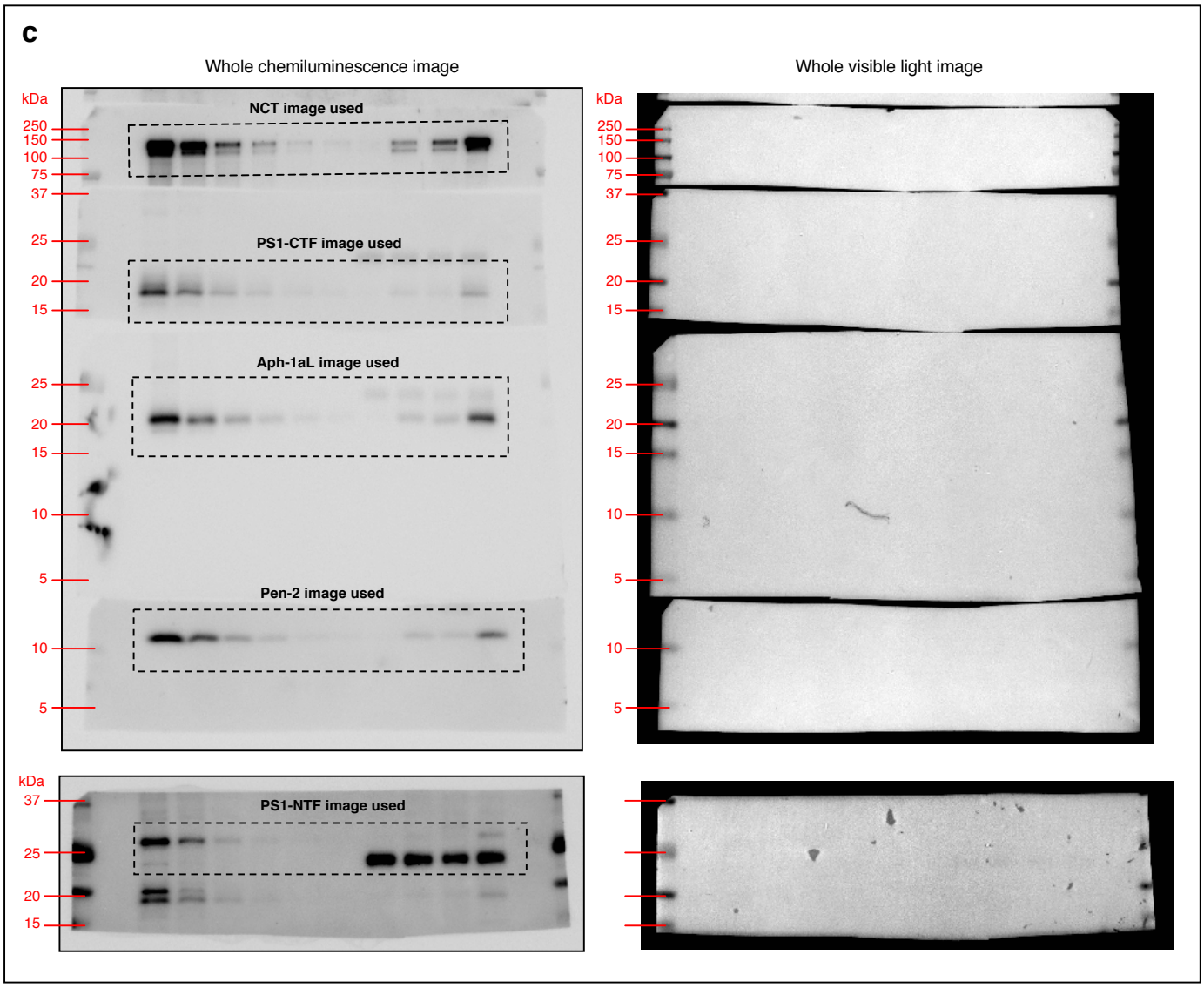

Supplementary Figure S17. Full scan images of Figure 5. Dashed rectangles indicate area used in Figure 5.

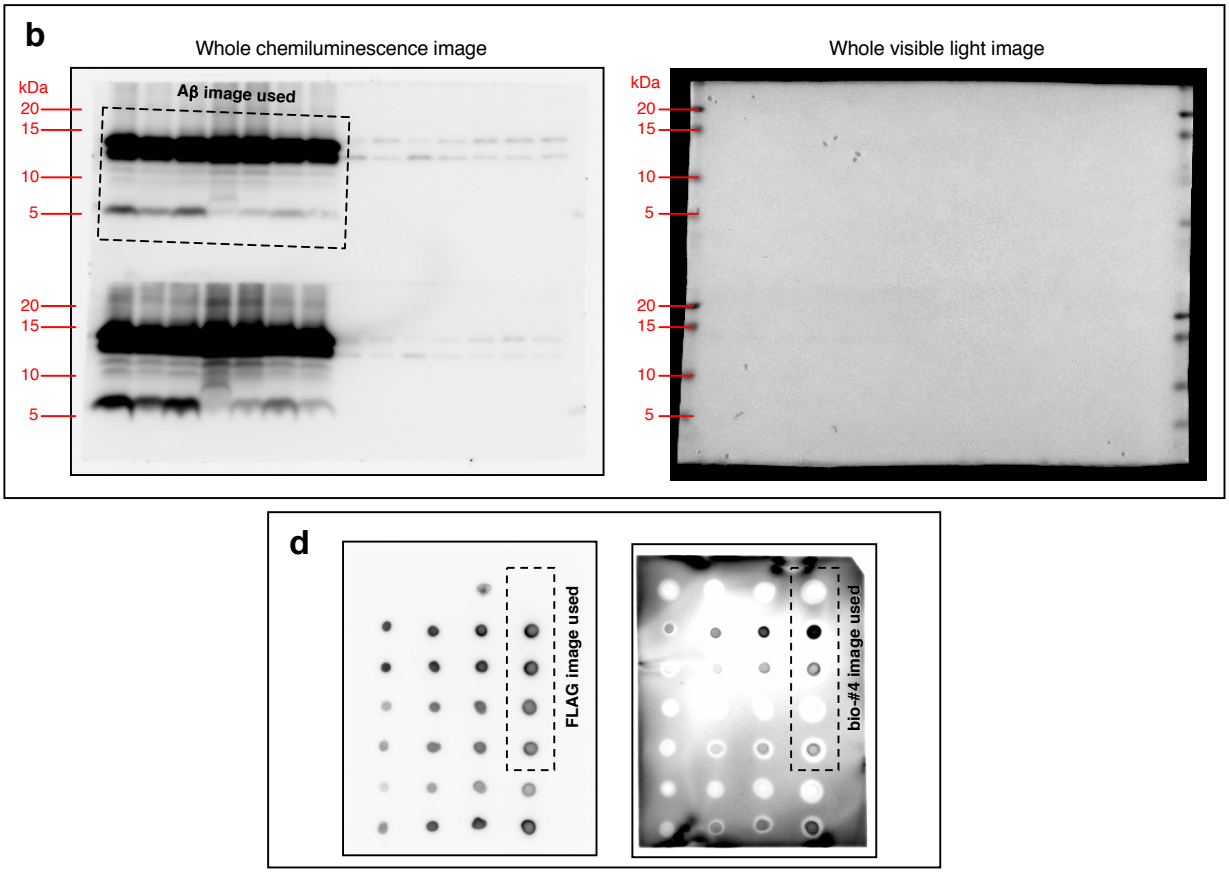

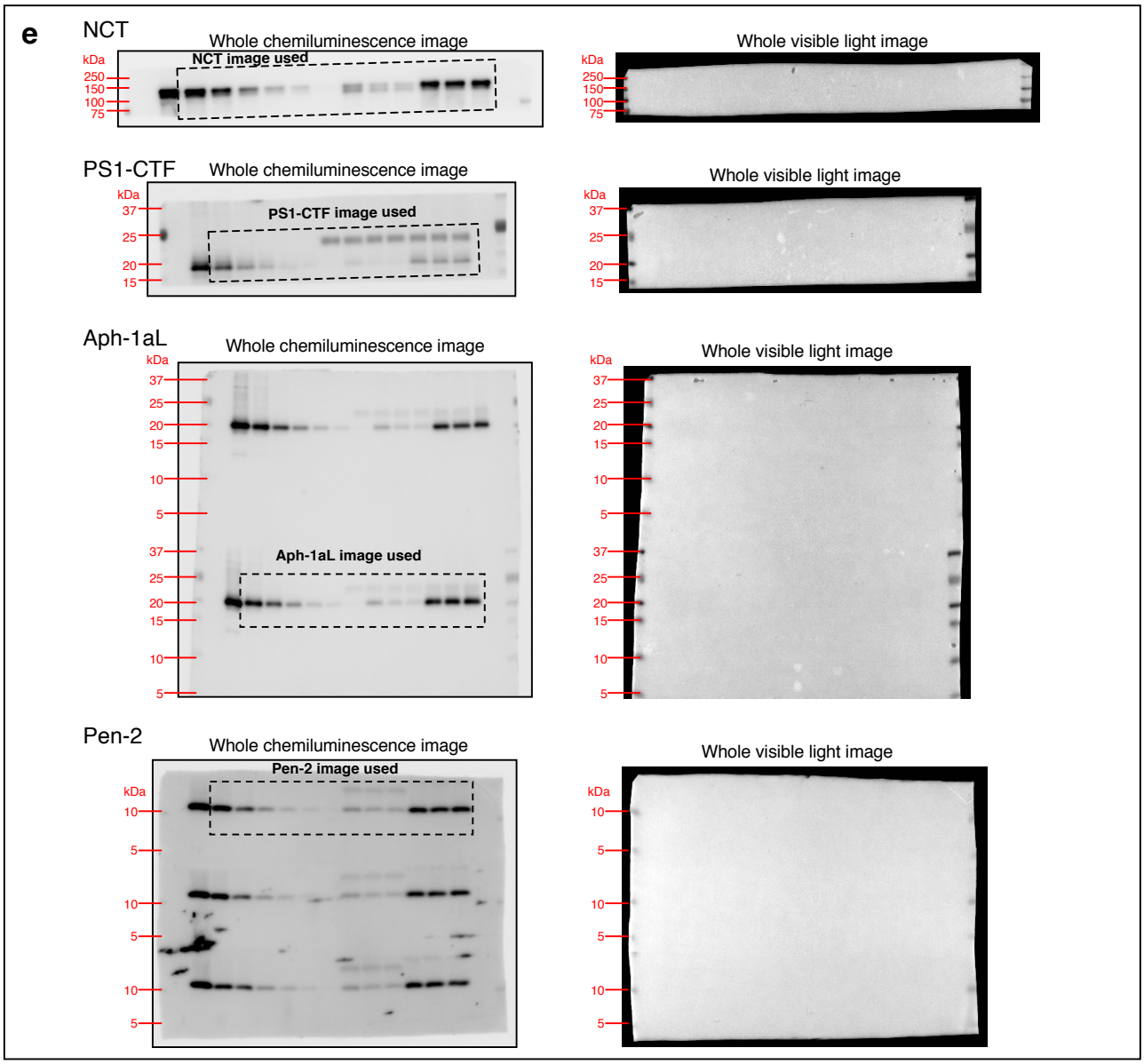

Supplementary Figure S18. Full scan images of Figure 6. Dashed rectangles indicate area used in Figure 6.

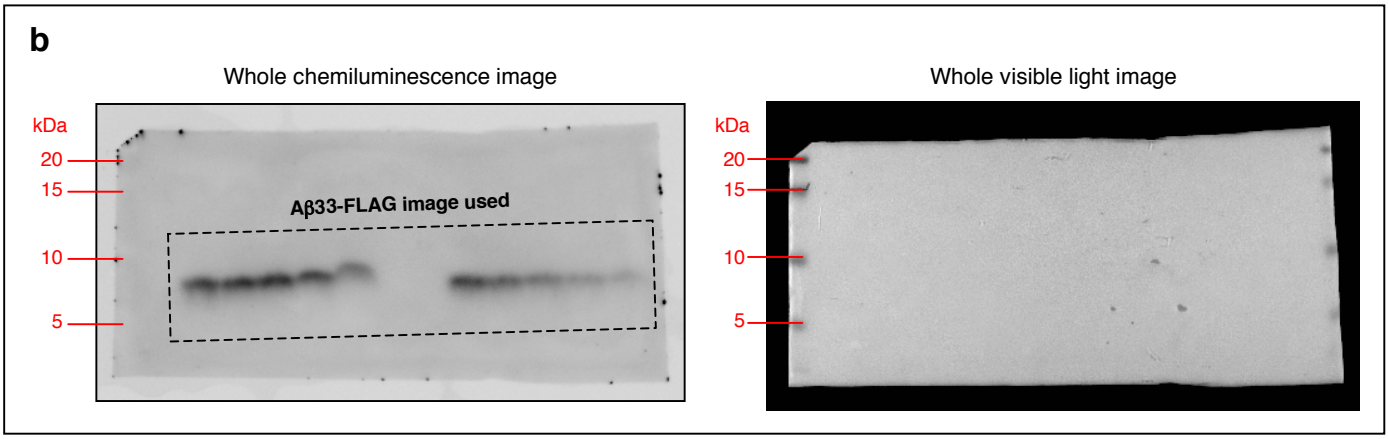

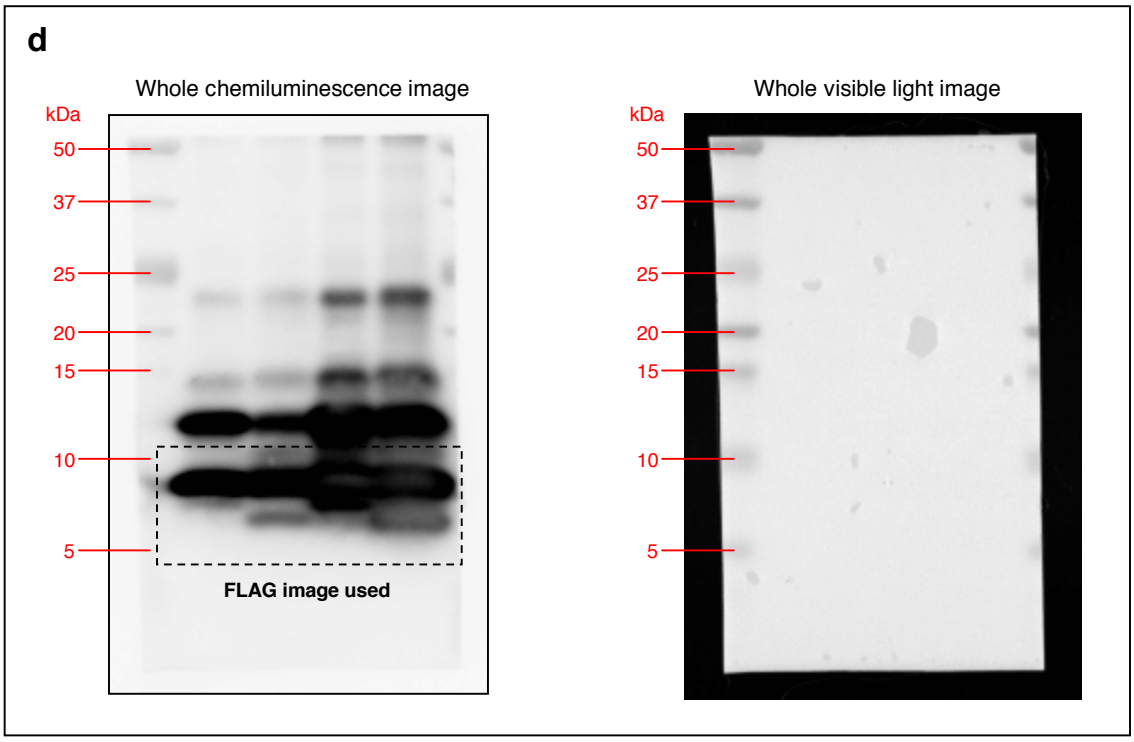

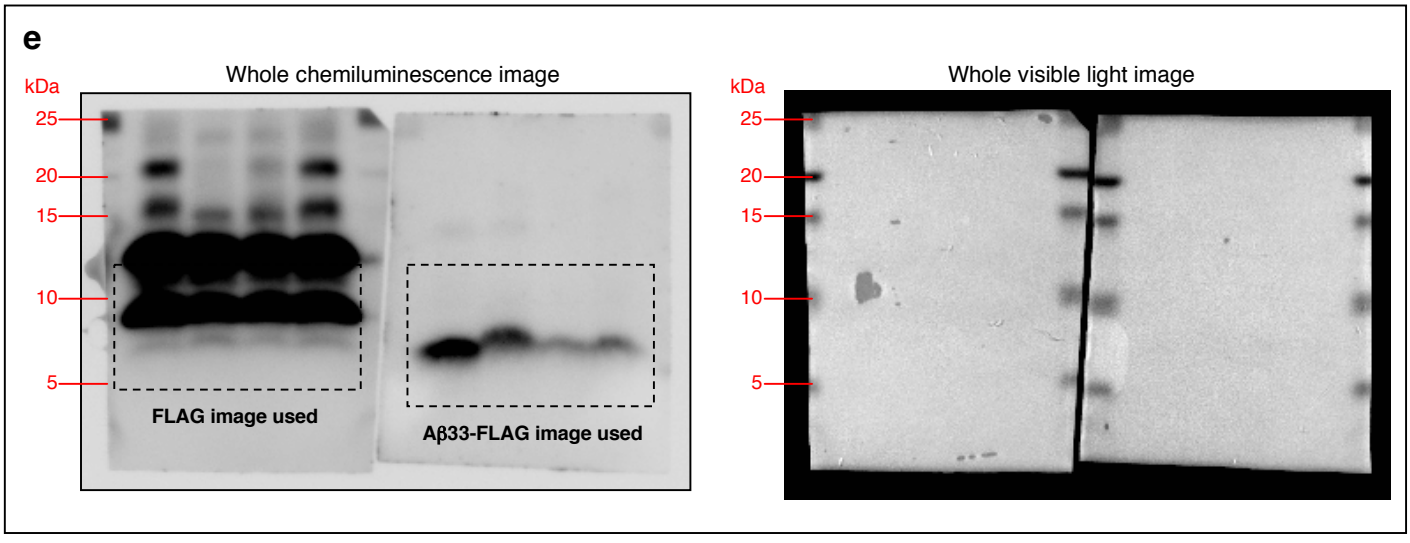

Supplementary Figure S19. Full scan images of Figure 7. Dashed rectangles indicate area used in Figure 7.

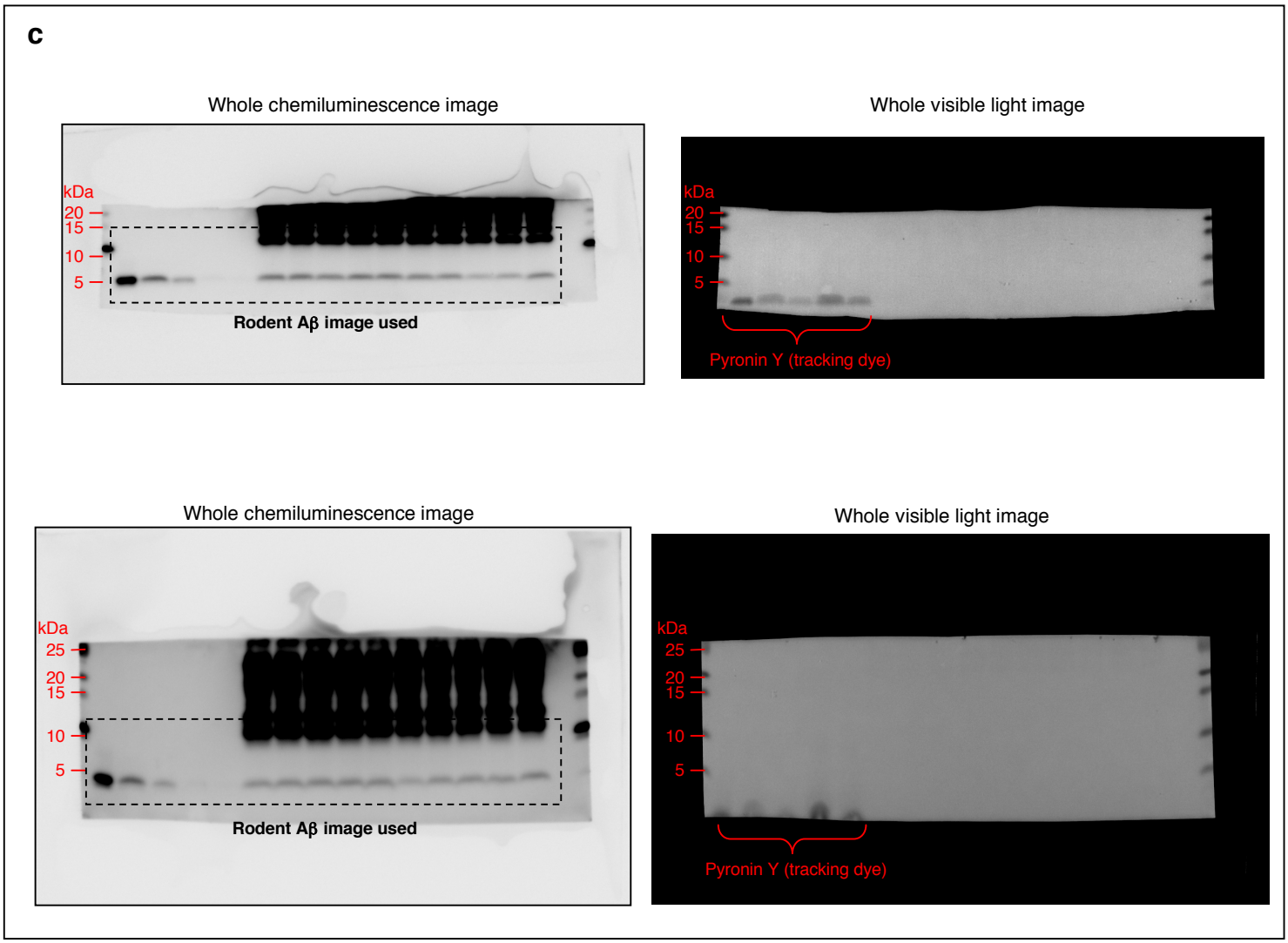

Supplementary Figure S20. Full scan images of Figure 8. Dashed rectangles indicate area used in Figure 8.

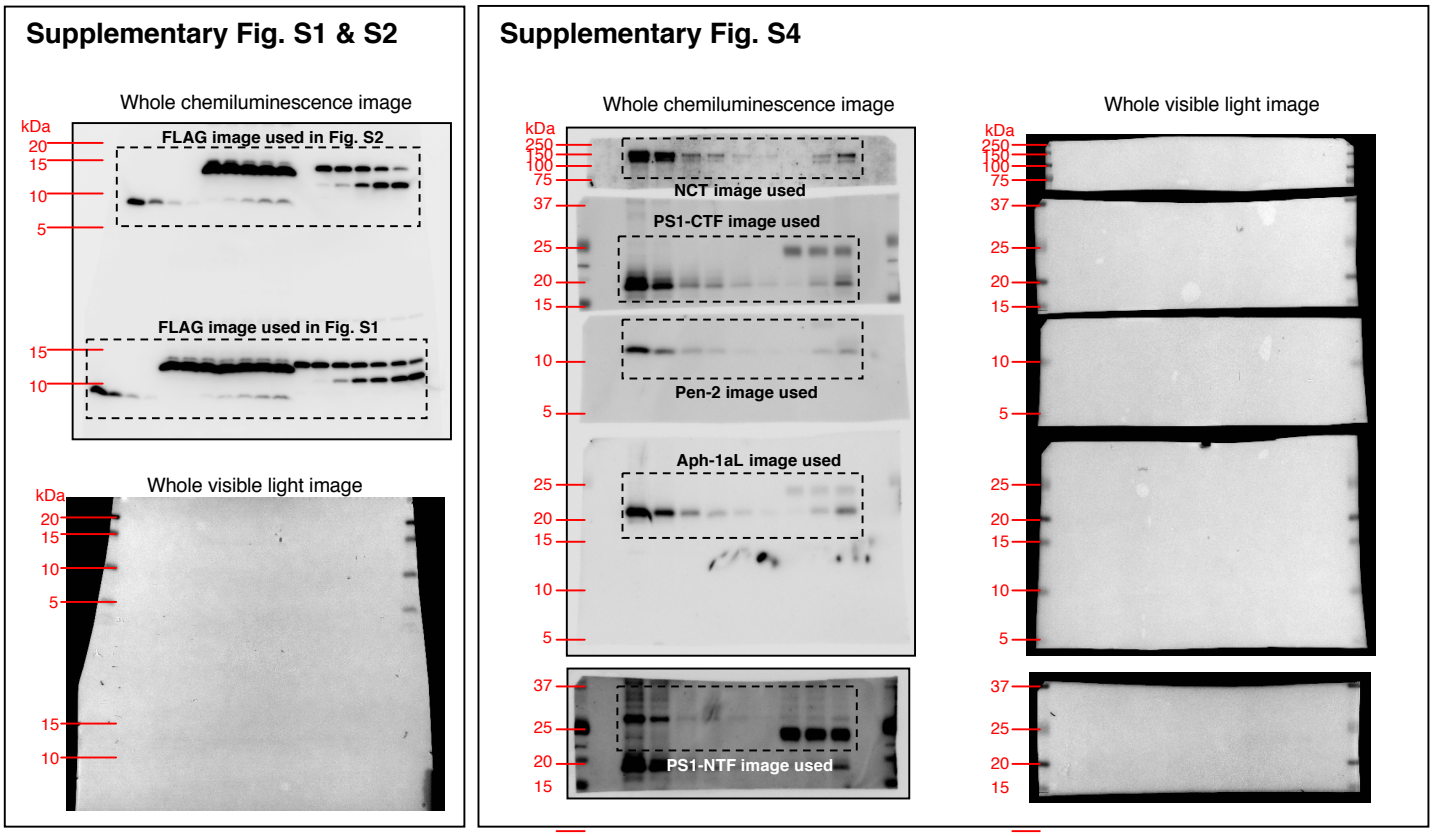

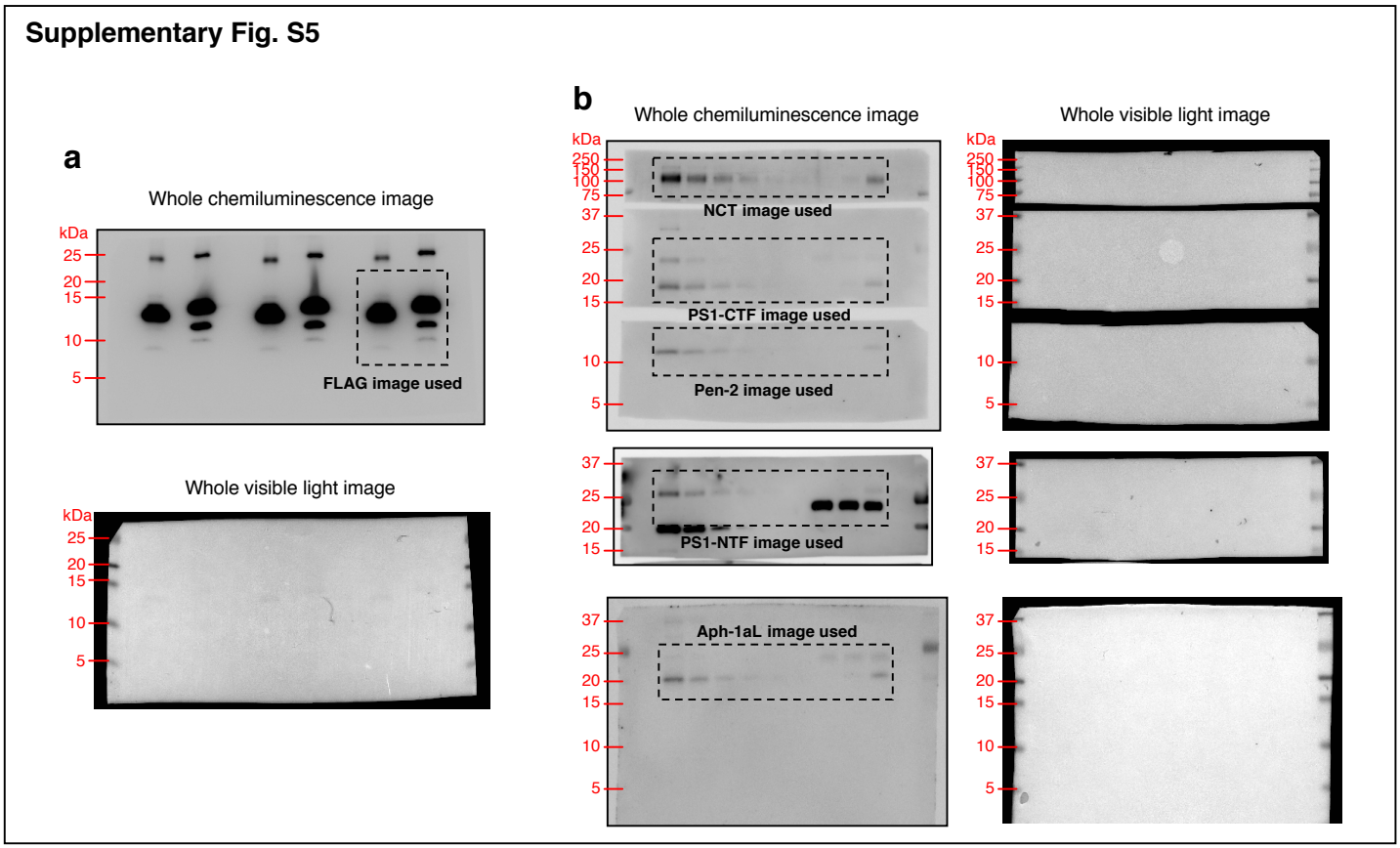

Supplementary Figure S21. Full scan images of Supplementary Figures S1, S2, S4 and S5. Dashed rectangles indicate area used in the Figures.

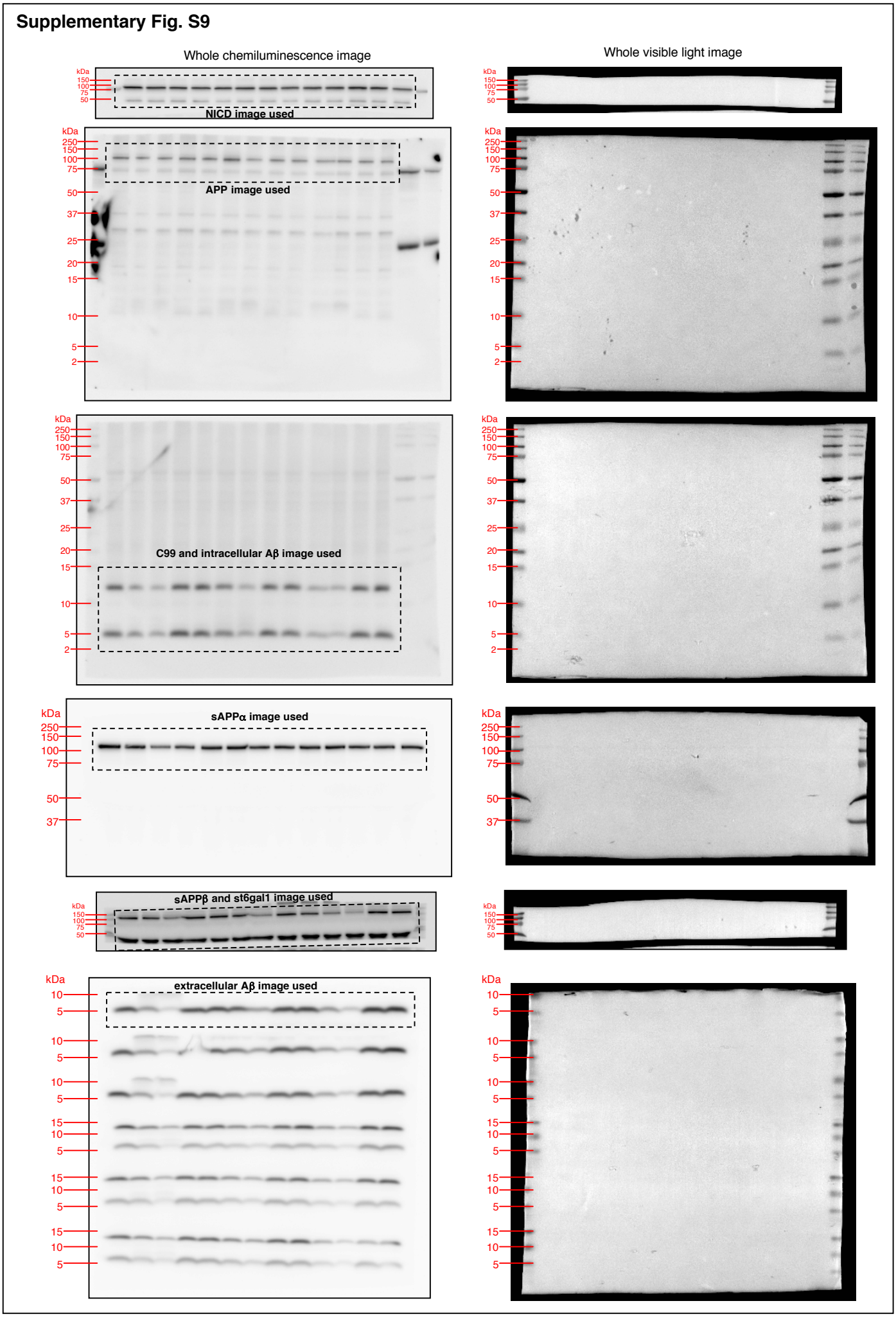

Supplementary Figure S22. Full scan images of Supplementary Figure S9. Dashed rectangles indicate area used in the Figure.

Supplementary Fig. S10

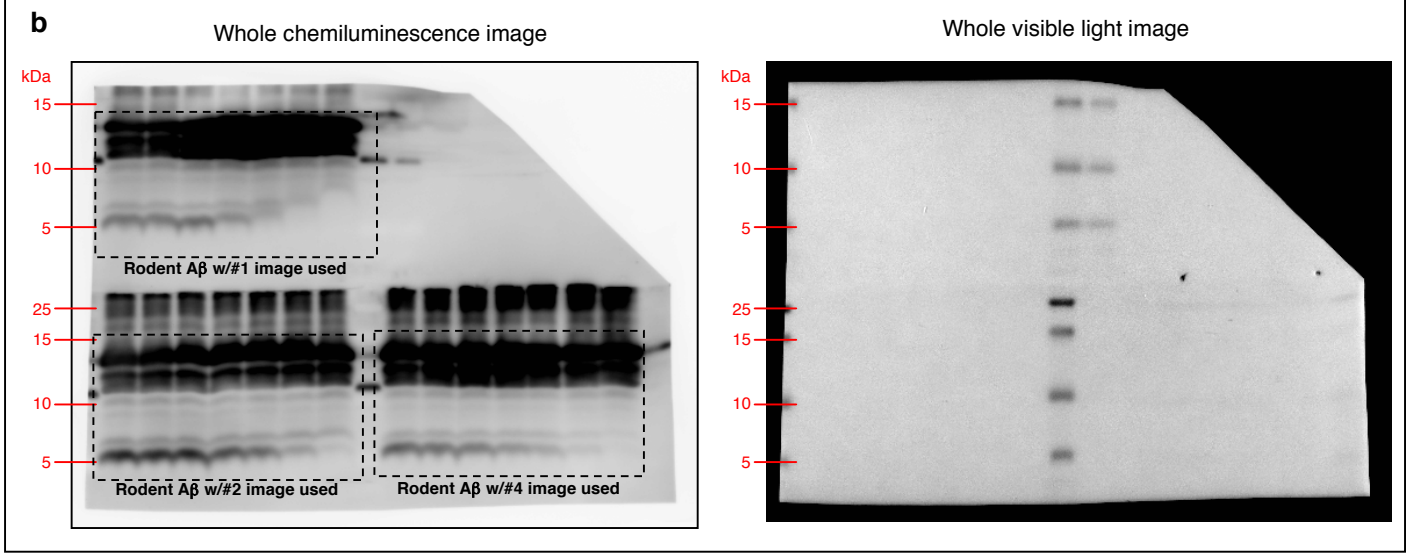

Supplementary Fig. S11

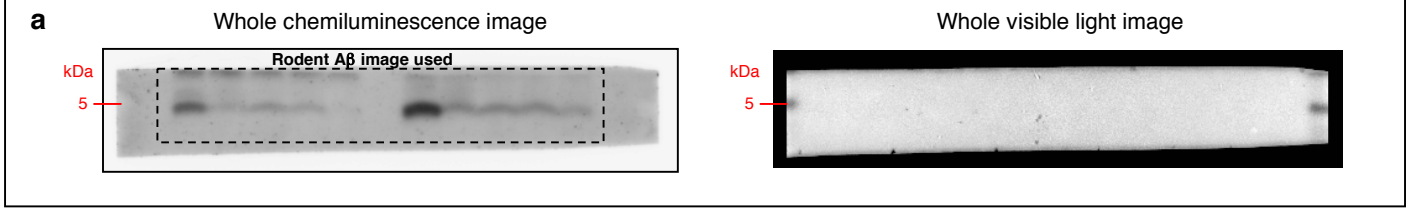

Supplementary Fig. S13

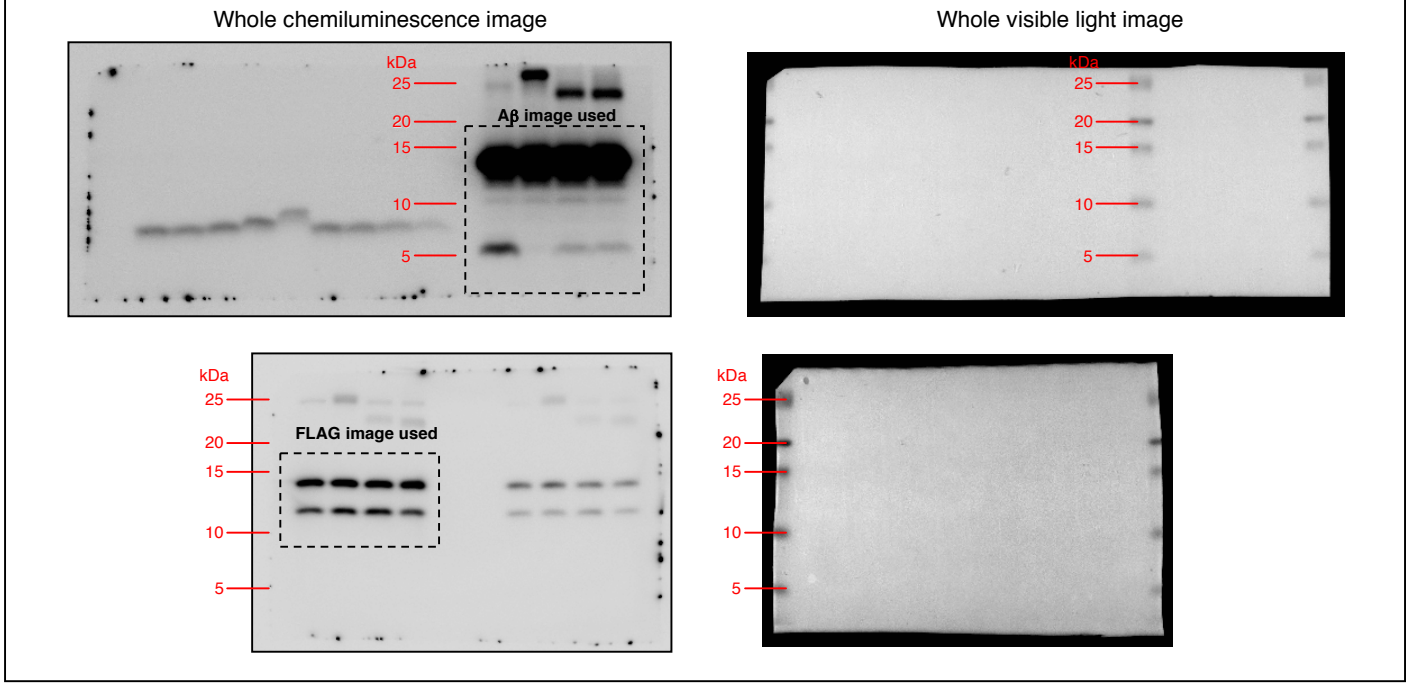

Supplementary Figure S23. Full scan images of Supplementary Figures S10, S11 and S13. Dashed rectangles indicate area used in the Figures.